Title:

Validation of the Aura Microwave Limb Sounder Temperature and Geopotential Height Measurements.

Submitted to: JGR-Atmospheres

Author list w/ email addresses:

Michael J. Schwartz	Michael@mls.jpl.nasa.gov
Alyn Lambert	alyn.lambert@jpl.nasa.gov
Gloria Manney	manney@mls.jpl.nasa.gov
William G. Read	bill@mls.jpl.nasa.gov
Nathaniel Livesey	livesey@mls.jpl.nasa.gov
Lucien Froidevaux	Lucien@mls.jpl.nasa.gov
Chi O. Ao	chi.o.ao@jpl.nasa.gov
Peter F. Bernath	pfb500@york.ac.uk
Chris Boone	cboone@acebox.uwaterloo.ca
Richard E. Cofield	rick@mls.jpl.nasa.gov
William H. Daffer	William.H.Daffer@jpl.nasa.gov
Brian Drouin	brian.j.drouin@jpl.nasa.gov
Eric J. Fetzer	eric.j.fetzer@jpl.nasa.gov
Ryan A. Fuller	fuller@mls.jpl.nasa.gov
Robert F. Jarnot	jarnot@mls.jpl.nasa.gov
Jonathon H. Jiang	Jonathon.H.Jiang@jpl.nasa.gov
Yibo Jiang	ybj@mls.jpl.nasa.gov
Brian W. Knosp	brian.knosp@jpl.nasa.gov
Kirstin Krueger	kkrueger@ifm-geomar.de
J.-L. Frank Li	Juilin.F.Li@jpl.nasa.gov
Martin G. Mlynczak	Martin.G.Mlynczak@nasa.gov
Steven Pawson:	Steven.Pawson-1@nasa.gov
James M. Russell III	james.russell@hamptonu.edu
Michelle L. Santee	mls@mls.jpl.nasa.gov
William van Snyder	W.V.Snyder-101705@jpl.nasa.gov
Paul C. Stek	Paul.C.Stek@jpl.nasa.gov
Robert P. Thurstans	rpt@mls.jpl.nasa.gov
Adrian.M.Tompkins	Adrian.Tompkins@ecmwf.int
Paul A. Wagner	Paul.A.Wagner@jpl.nasa.gov
Kaley A. Walker	kwalker@atmosp.physics.utoronto.ca
Joe W. Waters	joe@mls.jpl.nasa.gov
Dong L. Wu	dong@mls.jpl.nasa.go

Abstract:

Global satellite observations of temperature and geopotential height (GPH) from the Microwave Limb Sounder (MLS) on the EOS Aura spacecraft are discussed. The precision, resolution and accuracy of the data produced by the MLS version 2.2 processing algorithms are quantified, and recommendations for data screening are made. Temperature precision is 1 K or better from 316 hPa to 3.16 hPa, degrading to < 3 K at 0.001 hPa. The vertical resolution is 3 km at 31.6 hPa,

degrading to 6 km at 316 hPa and to < 13 km at 0.001 hPa. Comparisons with analyses (GEOS-5, ECMWF, MetO) and other observations (CHAMP, AIRS/AMSU, SABER, HALOE, ACE, radiosondes) indicate that MLS temperature has persistent, pressure-dependent biases which are between -2.5 K and +1 K between 316 hPa and 10 hPa. The 100 hPa MLS v2.2 GPH surface has a bias of < 150 m relative to the Goddard Earth Observing System version 5.0.1 (GEOS-5) values. These biases are compared to modeled systematic uncertainties. GPH biases relative to correlative measurements generally increase with height due to an overall cold bias in MLS temperature relative to correlative temperature measurements in the upper stratosphere and mesosphere.

Popular Summary

Space-based observations are one of the main sources of information about the middle atmosphere, where more conventional measurement techniques are not feasible because of the difficulties of reaching this layer of the atmosphere. In order to determine temperature and height, radiances measured by sensors on satellites need to be inverted using complex algorithms that generally require knowledge of spectroscopic parameters, error characteristics of the instrument, and some a-priori knowledge about the likely state of the atmosphere.

This paper describes the retrievals algorithm used to determine temperature and height from radiance measurements by the Microwave Limb Sounder on EOS Aura. MLS is a "limb-scanning" instrument, meaning that it views the atmosphere along paths that do not intersect the surface – it actually looks forwards from the Aura satellite. This means that the temperature retrievals are for a "profile" of the atmosphere somewhat ahead of the satellite. Because of the need to view a finite sample of the atmosphere, the sample spans a box about 1.5km deep and several tens of kilometers in width; the optical characteristics of the atmosphere mean that the sample is representative of a tube about 200-300km long in the direction of view. The retrievals use temperature analyses from NASA's Goddard Earth Observing System, Version 5 (GEOS-5) data assimilation system as a priori states. The temperature retrievals are somewhat dependent on these a priori states, especially in the lower stratosphere.

An important part of the validation of any new dataset involves comparison with other, independent datasets. A large part of this study is concerned with such comparisons, using a number of independent space-based measurements obtained using different techniques, and with meteorological analyses. The MLS temperature data are shown to have biases that vary with height, but also depend on the validation dataset. MLS data are apparently biased slightly cold relative to correlative data in the upper troposphere and slightly warm in the middle stratosphere. A warm MLS bias in the upper stratosphere may be due to a cold bias in GEOS-5 temperatures.

Draft of MApril 12, 2007

Validation of the Aura Microwave Limb Sounder Temperature and Geopotential Height Measurements

M. J. Schwartz[1], A. Lambert[1], G. L. Manney[1,2], W. G. Read[1], N. J. Livesey[1], L. Froidevaux[1], C. O. Ao[1], P. F. Bernath[3,4], C. D. Boone[3], R. E. Cofield[1], W. H. Daffer[1], B. J. Drouin[1], E. J. Fetzer[1], R. A. Fuller[1], R. F. Jarnot[1], J. H. Jiang[1], Y. B. Jiang[1] B. W. Knosp[1], K. Krüger[11], J.-L. F. Li[1], M. G. Mlynczak[10], S. Pawson[8], J. M. Russell III [9], M. L. Santee[1], W. V. Snyder[1], P. C. Stek[1], R. P. Thurstans[1], A. M. Tompkins[12], P. A. Wagner[1], K. A. Walker[3,5], J. W. Waters[1], D. L. Wu[1]

Abstract. Global satellite observations of temperature and geopotential height (GPH) from the Microwave Limb Sounder (MLS) on the EOS Aura spacecraft are discussed. The precision, resolution and accuracy of the data produced by the MLS version 2.2 processing algorithms are quantified, and recommendations for data screening are made. Temperature precision is 1 K or better from 316 hPa to 3.16 hPa, degrading to $\sim$ 3 K at 0.001 hPa. The vertical resolution is 3 km at 31.6 hPa, degrading to 6 km at 316 hPa and to $\sim$ 13 km at 0.001 hPa. Comparisons with analyses (GEOS-5, ECMWF, MetO) and other observations (CHAMP, AIRS/AMSU, SABER, HALOE, ACE, radiosondes) indicate that MLS temperature has persistent, pressure-dependent biases which are between -2.5 K and +1 K between 316 hPa and 10 hPa. The 100 hPa MLS v2.2 GPH surface has a bias of $\sim$ 150 m relative to the Goddard Earth Observing System version 5.0.1 (GEOS-5) values. These biases are compared to modeled systematic uncertainties. GPH biases relative to correlative measurements generally increase with height due to an overall cold bias in MLS temperature relative to correlative temperature measurements in the upper stratosphere and mesosphere.

1. Introduction

The Microwave Limb Sounder (MLS) [*Waters et al.*, 2006] on the Aura spacecraft [*Schoeberl et al.*, 2006], launched on 15 July 2004 observes thermal microwave limb emission from many molecules, including O_2. This paper describes MLS measurements of temperature and geopotential height (GPH) that are produced by version 2.2 of the MLS data processing algorithms (v2.2). The precision and resolution of these measurements are discussed, and accuracy is estimated through comparison with validated correlative data sets and by modeling the impacts of measurement parameter uncertainties.

[1]Jet Propulsion Laboratory, California Institute of Technology, Pasadena, California, USA.
[2]Also at Department of Physics, New Mexico Institute of Mining and Technology, Socorro, New Mexico, USA.
[3]Department of Chemistry, University of Waterloo, Waterloo, Ontario, Canada.
[4]Now at Department of Chemistry, University of York, York, U.K.
[5]Now at Department of Physics, University of Toronto, Toronto, Canada.
[6]Climate Change Research Center, Institute for the Study of Earth, Oceans, and Space, University of New Hampshire, Durham, New Hampshire, USA.
[7]Harvard-Smithsonian Center for Astrophysics, Cambridge, Massachusetts, USA.
[8]Global Modeling and Assimilation Office, NASA Goddard Space Flight Center, Greenbelt, MD, USA.
[9]Hampton University, Hampton, VA, USA.
[10]NASA Langely Research Center, Hampton, VA, USA.
[11]Leibniz-Institute for Marine Sciences at Kiel University (IFM-GEOMAR), Kiel, Germany.
[12]The European Centre for Medium-Range Weather Forecasts, Reading, U.K.

Knowledge of the thermodynamic state of the atmosphere is fundamental to atmospheric dynamics, chemistry, and radiation. MLS measurements of temperature and GPH and the related assignment of tangent-point pressures (ptan) to individual limb-views are also critical steps in obtaining the measurement of atmospheric constituents.

The Microwave Limb Sounder (MLS) on NASA's Earth Observing System (EOS) Aura satellite measures $\sim$ 3500 vertical profiles per day along the sub-orbital track. Initial validation of the first publicly-available Aura MLS dataset, version 1.5 (v1.5), was presented by *Froidevaux et al.* [2006]. Here we report on the quality of the recently-released v2.2 temperature and GPH measurements.

The v2.2 measurement system is described in Section 2. In addition to providing a review of instrumental and orbital characteristics, this section includes guidelines for quality control screening of the v2.2 temperature and GPH products, documents their precision and spatial resolution, and quantifies known systematic error. Section 3 focuses on comparisons between MLS data and analyses, collocated satellite observations of temperature and GPH. Finally, section 4 summarizes all these findings, reports on remaining issues with the validation of these MLS data, and outlines plans for future versions of the products.

2. MLS Temperature and GPH Measurement Description

2.1. Overview of the MLS Measurement System

MLS observes thermal microwave emission by the atmosphere in five spectral regions from 118 GHz to 2.5 THz. The temperature and GPH measurements described in this paper are taken from observations near the 118-GHz O_2 spectral line and the 234-GHz $O^{18}O$ spectral line. MLS looks forward from the Aura spacecraft and scans the Earth's limb vertically from the ground to $\sim$90 km every 24.7 s. The vertical scan rate varies with altitude, with the slowest scan (giving a better signal to noise through greater integration time) used in the lower regions ($\sim$0 – 25 km). The MLS vertical scans are synchronized to the Aura orbit such that vertical scans are made at essentially the same latitudes each orbit, with 240 scans performed per orbit ($\sim$3500 scans per day).

This paper describes MLS 'Level 2' data, which are geophysical products reported along the measurement track of the instrument. These are retrieved from calibrated MLS radiance observations ('Level 1 data') by the MLS data processing software [*Livesey et al.*, 2006]. MLS Level 2 products are reported on a fixed vertical pressure grid. Most products use a grid having 6 levels per decade change in pressure in the troposphere and stratosphere, thinning out to 3 per decade at pressures less than 0.1 hPa. In v2.2, temperature, GPH and water vapor are retrieved on a higher-resolution grid in the troposphere and lower stratosphere, with 12 levels per decade from 1000 to 22 hPa. Retrieved profiles are evenly spaced at 1.5° great circle angle (geodetic) along the orbit track, giving 240 Level 2 profiles per orbit at fixed latitudes. There are approximately the same number of retrieved profiles as there are limb scans, but a block of limb scans is used to retrieve a block of profiles and an individual retrieved profile is not associate with a single limb scan.

The MLS Level 2 products are reported in Level 2 Geophysical Product (L2GP) data files. Individual files generally contain a single MLS 'standard product' (temperature, GPH, H_2O etc.) for a 24 hour period from midnight to midnight universal time. The L2GP files store the data in an HDF-EOS version 5 swath format with the swath name describing the product. In addition to "Temperature," the standard temperature file contains two swaths that are estimates of tropopause pressure, calculated using the WMO algorithm [*Reichler et al.*, 2003] on the MLS temperature and on Goddard Earth Observing System, version 5 (GEOS-5) temperature, respectively. The MLS Version 2.2 data quality document [*Livesey et al.*, 2007a] gives more information on the format and contents of the MLS data files.

Version 2.2 (v2.2) is the 2nd public release of MLS data and has been used to process the incoming data stream since March 2007. Reprocessing of data collected since MLS became operational in August 2004 is also in progress using the v2.2 algorithms. These processing streams have the specific version name v2.21 and include a minor software patch applied to an earlier version v2.20 that corrects the handling of MLS Level 1 radiances flagged as bad data. We refer to both these versions collectively as version 2.2 (v2.2). For this validation effort, 93 days of v2.20 data covering late 2004 to early 2007 were processed with an emphasis on special months or days of interest for validation (including campaigns).

2.2. Temperature and GPH

The MLS measurement system [*Livesey et al.*, 2006] uses optimal estimation theory [*Rodgers*, 2000] to retrieve a state vector parameterizing the estimated atmospheric state. The v2.2 atmospheric "state vector" includes temperature on 47 pressure levels (not all of which are retrieved) and GPH on the 100-hPa surface (refGPH.) Given these 48 pieces of information, the other GPH levels are determined through assumed hydrostatic balance and knowledge of the molar mass of air. The state vector also includes the tangent pressures (ptan) of the limb observations, which link MLS pointings to the pressure surfaces on which values are retrieved. These state vector elements are interrelated through the instrument

scan model and through assumed hydrostatic balance, and are simultaneously retrieved.

The temperature/GPH/ptan retrieval uses radiances and estimated radiance precisions from measurements made in the vicinity of two O_2 spectral lines (discussed in Section 2.5) along with a scan model (antenna pointing and atmospheric refraction), a field-of-view model based upon pre-launch measurements, a priori estimates of temperature and 100-hPa refGPH (with appropriately conservative uncertainties) a smoothing model (Tikhonov regularization) and a forward model (the function that simulates radiances given a state vector.) A state vector is found that minimizes χ^2, which is the sum of the squared differences between observations and simulated observation divided by the squared measurement precisions.

Geopotential, Φ, is gravitational acceleration, $g(\phi,h)$, integrated with respect to geometric height, h, from the mean-sea-level reference geoid. GPH is obtained by dividing geopotential by a standard sea-level gravity; it has units of length, but its "meter stick" varies with latitude and height. Given the assumptions of atmospheric hydrostatic balance and the ideal gas law, GPH can be recast as the integral of temperature with respect to log pressure:

$$\mathrm{GPH} \equiv \frac{1}{g_0}\int g\,dh = \frac{R}{Mg_0}\int T\,d(-\ln P),$$

where R is the gas constant and M is the molar mass of air. The use of GPH as a vertical coordinate eliminates centrifugal force and air density from the primitive equations which describe hydrodynamical flow of the atmosphere [e.g., *Brasseur and Solmon*, 1986]. GPH contours on surfaces of constant pressure are stream functions for geostrophic winds.

MLS measures thermal emission from the atmosphere, which depends upon how warm and how opaque the atmosphere is along a limb path. All MLS measurements contain temperature information, but opacity near trace-gas spectral lines also depends upon trace gas abundance. This dependence permits retrievals of trace-gas abundances but confounds the temperature retrieval. Diatomic oxygen (O_2), on the other hand, has a known atmospheric isotopic ratio and mixing ratio, so bands in spectral regions where O_2 is the predominant source of opacity are used to determine temperature, GPH and ptan.

MLS gets temperature information from both "saturated" (optically thick) and "unsaturated" (optically thin) limb radiances. When viewing along limb paths and at frequencies where the atmosphere is opaque, radiances are "saturated" at a weighted average of the black-body emission from some layer of the atmosphere. In this limit, a single channel/pointing provides temperature information about some layer of the atmosphere. Observations with multiple channels of "unsaturated" radiances near pressure-broadened O_2 lines provide estimates of limb-tangent pressure (ptan) from line shape. These measurement of pressure as a function of limb-pointing height (from the antenna/spacecraft scan model,) also determine temperature through assumed hydrostatic balance.

The a priori temperature used in the MLS v2.2 retrieval between the surface and 1 hPa is the GEOS-5 analysis, discussed in Section 3.1. At levels above 1 hPa, CIRA86 climatology [*FLEMING et al.*, 1990] is used. There is a $\sim$ 5-km layer at 1 hPa over which the two sources of a priori transition smoothly. The assumed a priori temperature precision is piecewise linear in log of pressure: 5 K at 1000 hPa, 10 K at 220 hPa and 20 K at 68 hPa and lower pressures. The a priori refGPH (GPH at 100 hPa) is 16 km and its precision is 5 km. Assumed a priori precisions are chosen conservatively, (loosely) so that a priori information is weighted less heavily than information from measured radiances.

2.3. MLS Temperature and GPH Data Usage Guidelines

In addition to describing file formats and contents, the data quality document [*Livesey et al.*, 2007a] also gives detailed instructions on the proper use of all MLS data products. The pertinent information, which is identical for MLS temperature and GPH, is repeated here.

Each MLS Level 2 data point is reported with a corresponding precision value that quantifies the impact of radiometric noise and of uncertainty in the a priori. If the retrieval does not improve precision (reduce its value) by a factor of two from its a priori value, then it has failed to extract additional information from radiances and retrieved values will be significantly influenced by a priori. As an aid to users, the precisions of these retrieved values are set negative and these data are not recommended for use in scientific studies. There is further discussion of temperature and GPH precision in Section 2.6.

Three additional data flags are provided for every vertical profile. "Status" is a bit field indicating operational abnormalities or problems with the retrievals. The meanings of its bits are given in Table 1. Profiles for which Status is an odd number should not be used in any scientific study. Nonzero but even values of Status indicate that the profile has been marked as questionable by the data processing software, usually because measurements are possibly affected by the presence of clouds. At pressures of 147 hPa and lower (higher in the atmosphere), the cloud bits may generally be ignored. In the troposphere an attempt has been made to screen out radiances that have been influence by clouds, but some cloud-induced negative biases in retrieved temperature

Table 1. Meaning of bits in the 'Status' field.

Bit	Value[a]	Meaning
0	1	Flag: Do not use this profile (see bits 8–9 for details)
1	2	Flag: This profile is 'suspect' (see bits 4–6 for details)
2	4	Unused
3	8	Unused
4	16	Information: This profile may have been affected by high altitude clouds
5	32	Information: This profile may have been affected by low altitude clouds
6	64	Information: This profile did not use GEOS-5 temperature a priori data
7	128	Unused
8	256	Information: Retrieval diverged or too few radiances available for retrieval
9	512	Information: The task retrieving data for this profile crashed (typically a computer failure)

[a]The 'Status' field in an L2GP file is the total of appropriate entries in this column.

of up to 10 K are still evident, particularly in the tropics. Clouds which are along the limb path between the spacecraft and the tangent point have been found to have larger impacts on the retrieval than those near the tangent point. Temperatures in the tropopause (316 hPa–178 hPa) should be rejected as possibly influenced by cloud if the low-cloud Status bit is set in either of the two profiles following the profile in question. The flagging of clouds is discussed in more detail in Section 2.4.

The "Quality" field indicates the degree to which the measured MLS radiances have been fitted by the Level 2 algorithms. Larger values of Quality generally indicate better radiance fits, whereas values closer to zero indicate poorer radiance fits, and thus less reliable data. The Quality reported with the v2.2 temperature is based only upon the χ^2 of Band 8 radiances (radiances used in the temperature retrieval are discussed in Section 2.5) and so is primarily an indication of the fit of the retrieval in the troposphere. However, low values of Quality are not consistently associated with profiles that are outliers. As a precaution, against using data where the retrieval has not been able to fit the radiances, profiles having Quality values less than 0.6 are generally not recommended for scientific use. This threshold for Quality typically excludes ~4% of temperature profiles.

Additional information on the success of the retrieval is conveyed by the "Convergence" field, which is a measure of how well the retrieval algorithm has fit the radiances used in a 'chunk' of ~10 profiles. Values around 1.0 typically indicate good convergence. Use of profiles with Convergence greater than 1.2 is not recommended for scientific studies. Rejecting profiles with Convergence greater than 1.2 typically rejects 2 percent of profiles, and only 0.5 percent that have not already been screened out by Quality less than 0.6. Temperature and GPH at pressures lower than 0.001 hPa or higher than 316 hPa are not recommended for use in scientific studies. Unlike in v1.5, these levels are not, as a rule, marked with negative precision. Precision is set negative when it reaches half of its a priori value, indicating that half of the information is coming from a priori. However, the constraint on smoothness of retrieved profiles (implemented as Tikhonov constraint of curvature described in *Livesey and Snyder* [2004]), gives the retrieval confidence in its ability to extrapolate to levels beyond where it has radiance information. χ^2 doesn't increase to the point where the retrieval is considered to be over-influenced by a priori because the information is coming, not from a priori, but from smoothing. A better method of setting negative precision, which also flags profiles too-heavily based upon extrapolation, will be added to any future version of the MLS level 2 algorithms.

A special case of low Quality (between 0.4 and 0.55) and high (poor) convergence has been identified poleward of 70° latitude in the polar autumn and early winter. Figure 1 shows such a cluster of points in data from four days in April and May of 2006. For this group of days, more than half of profiles south of 70° S have Quality less than 0.6. Figure 2, shows retrieved temperature minus a priori for selected levels for a similar case in northern-hemisphere autumn. Here, Quality and Convergence reflect the convergence failure in the final "phase" of the temperature retrieval, which attempts to combines radiances from the isotopic $O^{18}O$ line at 234 GHz with radiances from the vicinity of the 118-GHz O_2 line. This behavior is believed to be related to the impact of O_3, which is not properly retrieved or constrained in this phase, and will be addressed in any future retrieval version. In these cases, the retrieved state falls back to the generally well-behaved output of a previous "phase" that uses only 118-GHz radiances and has somewhat degraded vertical resolution in the troposphere. Bi-

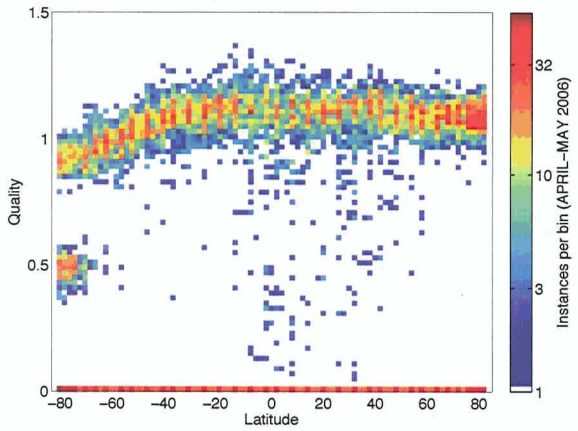

Figure 1. Temperature Quality flag for April–May, 2006. There is a group of points in the southern autumn, south of 70° S, which have Quality less than 0.7. These are cases where the final "phase" of the temperature retrieval failed to converge, and the retrieval reverted to the result of an earlier "phase." A similar group of retrievals is seen in the northern autumn, 12-Nov-2004.

ases between the standard temperature product and the output the earlier phase (Temperature-UpdatePtan) are generally less than 1 K in the stratosphere and, in studies of polar processes in the stratosphere, it may be useful to relax the Quality threshold to 0.4 to fill in gaps in maps. The highest pressure retrieved (lowest height) in the "UpdatePtan" phase is 261 hPa, and the 261 hPa level itself should not be used in scientific studies. At latitudes south of 70° N, Figure 1 exhibits behavior typical of other days, with low values of Quality generally near profiles that are affected by clouds, but not necessarily exactly marking profiles that are obvious outliers from a priori.

In summary, the following data-quality screens should be applied when using MLS v2.2 temperature and GPH data. The data should be used only when:

1. The precision value for that data point is positive
2. The Status field for that profile is an even number
3. The Quality field for that profile is greater than 0.6. A Quality threshold of 0.4 may be used in studies of the polar stratosphere.
4. The Convergence field is less than 1.2.
5. Status bit 5 (low cloud) is not set in either of the two subsequent profiles. The last two profiles of a day cannot be flagged with this method and should not be used in the troposphere. The low-cloud bits may be ignored at retrieval levels with pressures less than 178hPa.

2.4. Impact of Clouds on MLS Temperature

MLS observations are unaffected by thin cirrus clouds or stratospheric aerosols, however thick clouds associated with deep convective thunderstorms can have an impact on the MLS radiances. The effect of emission and scattering from high altitude clouds (~200 hPa) is to enhance the MLS radiance signals, while scattering by low clouds leads to suppression of observed limb radiances. These signatures are generally fairly spectrally flat. However, large amounts of scattering from the thickest clouds can attenuate the spectral variations in MLS radiances on which the temperature measurements are based. The MLS data processing algorithms retrieve a spectrally flat 'extinction' term to compensate for scattering by moderate clouds. When the algorithms detect particularly thick clouds that significantly affect the spectral contrast (through comparison of the observed radiances with predictions from a clear-sky-only radiative transfer model) radiances from individual 1/6 s MLS integration periods are omitted from the retrieval.

MLS v2.2 temperature at the highest retrieved pressures (316–216 hPa) contains negative outliers of up to ~ 10 K due to the imperfect screening of radiances impacted by thick low clouds. Figure 2 shows such outliers in differences between MLS v2.2 and a priori temperatures, with red points showing the points flagged as possibly-cloudy by the time-shifted low-cloud-bit method recommended in Section 2.3. These outliers are particularly evident in the tropics, both because of its deeper convection and small variability of temperature. Figure 3 shows the probability distribution function (PDF) of the difference between MLS and GEOS-5 temperature at 316 hPa in the tropics (−20° to 20°) as a solid black line. An asymmetric tail of negative values is evident. The dashed black line on the plot is the positive side of the distribution folded over at the place which gives the best match of folded-positive and negative distributions within half of a standard deviation (σ) from the peak. The solid black line on the high side and the dashed on the low side form a cloud-cleared PDF, and the difference between the black solid and dashed lines, shown in red, is the PDF of the negative, cloud-induced tail. The magenta vertical line is 2σ below the peak of the symmetrized distribution.

In these tropical profiles, 12 percent of profiles at 316 hPa are in the tail and more than 2σ from the cloud-cleared mean. This tail magnitude is 10 percent at 261 hPa, 11 percent at 215 hPa and 9 percent at 178 hPa. At 147 hPa, the magnitude of the tail drops to ~ 1.5 percent, and the technique of folding the distribution produces a difference that is primarily asymmetry close to the center rather than a negative tail.

The PDFs of three cloud-flagging methods are also shown

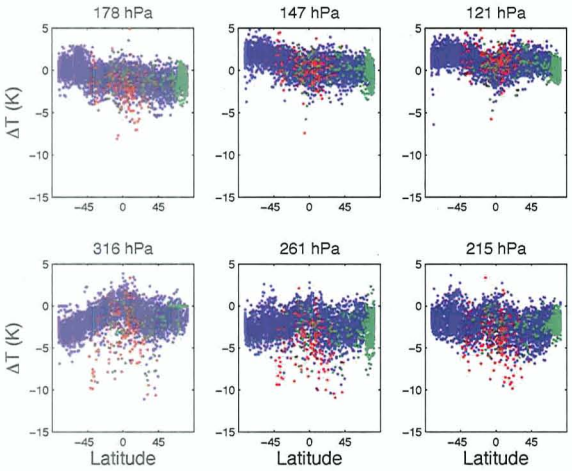

Figure 2. MLS v2.2 temperature minus GEOS-5 a priori from November 12,2004, showing Quality and cloud flagging. The red points are points for which the low-cloud bit of "Status" is set in one of the two subsequent profiles. Green points have Quality < 0.6.

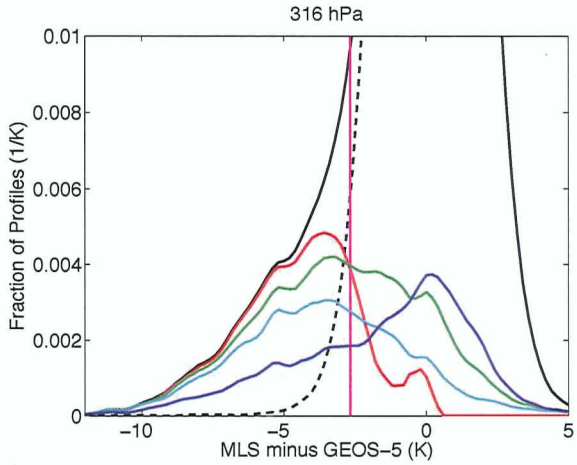

Figure 3. Cloud-flagging at 316 hPa in the tropics (20°N to 20°S). The solid black curve is the PDF of MLS minus GEOS-5 temperature. The dashed black line is the positive side of the distribution folded over at the point which gives the best match with the negative side within $\pm 1\sigma/2$ of the distribution center. The red line is the difference between the solid black and dashed black lines, taken to be the PDF of the negative, cloud-induced outliers. The magenta vertical line is 2σ below the cloud-cleared distribution center (0.2 K - 2.9 K). The blue line is the PDF of profiles flagged using the low-cloud flag of the current profile. The cyan line is the PDF of profiles flagged using the low-cloud flag from two profiles later than the current profile. The green line is the PDF using the recommended cloud screening, the low cloud flag from either of the two subsequent profiles.

in Figure 3. The dark blue line is the PDF from using the low-cloud bit of the current profile. The cyan line uses the low-cloud bit from two profiles after the current profile. The green line is the PDF obtained if either of the following two profiles has its low-cloud bit set. Ideally, a cloud flag looks something like the red, cloud-induced tail, identifying the outliers without rejecting other parts of the distribution. The third method (green line), which is the recommended screening, captures 88 percent of the part of the 12 percent of total profiles that are more than 2σ from center in the negative tail. It also falsely flags 5 percent of profiles that are more positive than 1 σ below the cloud-cleared mean as cloudy. The unshifted low-cloud flag (dark blue) is successful at capturing only 38 percent of the tail with a 6 percent false positive rate. Using the high and low-cloud flags shifted by one and two profiles (not shown) captures 96 percent of the tropical negative tail, but flags 42 percent of total tropical profiles as cloudy. At 178 hPa, the recommended screening captures 76 percent of the negative tail with a 9 percent false positive rate.

Clouds generally have little impact upon retrieved temperature at 100 hPa or lower pressures, however there are some cases in which clouds are associated with oscillatory behavior in temperature profiles into the stratosphere. Distinguishing possible retrieval instability from atmospheric variability (such as gravity waves) is an area of research.

2.5. Radiance Spectra and Radiance Residuals

Figures 4, 5, 6, and 9 show typical MLS radiances in the vicinity of the 118-GHz O_2 line and Figure 8 shows those in the vicinity of the $O^{18}O$ line at 234 GHz. MLS band 22 provides radiances within ± 4 MHz of the 118-GHz line center with 100 kHz resolution. Band 1 provides radiances within ± 575 MHz of the 118-GHz line center with channel bandwidths ranging from 6–96 MHz. Bands 32 and 34 have 500-MHz wide channels centered 1.75 GHz and 3.5 GHz from the 118-GHz line center. Band 8 has channels within ± 575 MHz of the 234-GHz line center with channel bandwidths ranging from 6–96 MHz. Band 33 channel 3 has 500-MHz passbands at 232.5 GHz and 246.9 GHz. Emission in these spectral regions is dominated by oxygen, and is used to infer limb tangent-point pressures of MLS observations and to derive MLS temperature and GPH. The O_2 mixing-ratio is assumed constant from the surface to 0.008 hPa [*Schwartz et al.*, 2006].

The MLS "Core" retrieval uses an optimal estimation approach [*Rodgers*, 2000; *Livesey et al.*, 2006] on these radiances to produce estimates of temperature, geopotential height and tangent pressure. The lower parts of Figures 4, 5 6 9, 8, show the average fits achieved to these measured radiances by the retrieval algorithms. The scatter about these averages (not shown) is generally consistent with the levels of noise seen in the radiances, as is expected and desired.

The fits for the saturated channels of Band 1, shown in Figure 4, are generally within ~0.3 K. The outer channels of Band 1, which are used in the mid-stratosphere and

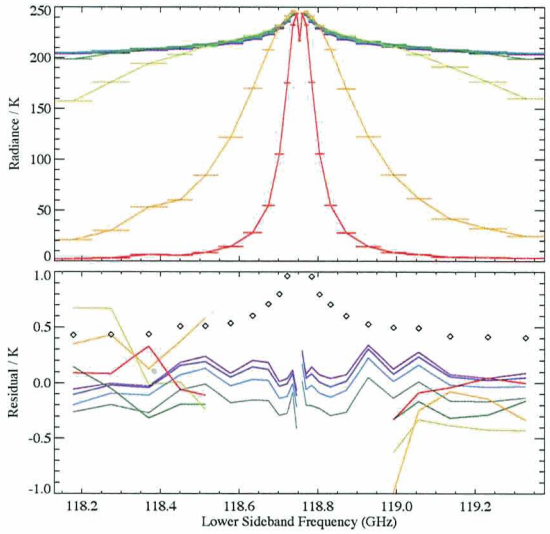

Figure 4. Top: sample radiances (in units of brightness temperature) from the MLS Band 1, centered on the 118 GHz O_2 line. Global average radiances from observations on 24 September 2004 are shown for eight scan positions with approximate tangent altitudes: ~7.5 km (purple), ~11 km (dark blue), ~15 km (light blue), ~18 km (dark green), ~22 km (light green), ~26 km (yellow green), ~36 km (orange), ~46 km (red). This is a single-sideband radiometer, so all radiances are from below the 126-GHz local oscillator. These radiances are the primary source of MLS temperature in the stratosphere and lower mesosphere. The widths of the various MLS spectral channels are denoted by the horizontal bars. (Bottom:) The average fit achieved to these radiances by the MLS v2.2 retrieval algorithms. The v2.2 retrieval does not use channels 6–20 for limb-pointings with tangent pressures less than 50 hPa, so these channels do not have residuals for the four highest-altitudes shown. Diamonds are radiance precisions used in the retrievals χ^2 calculations.

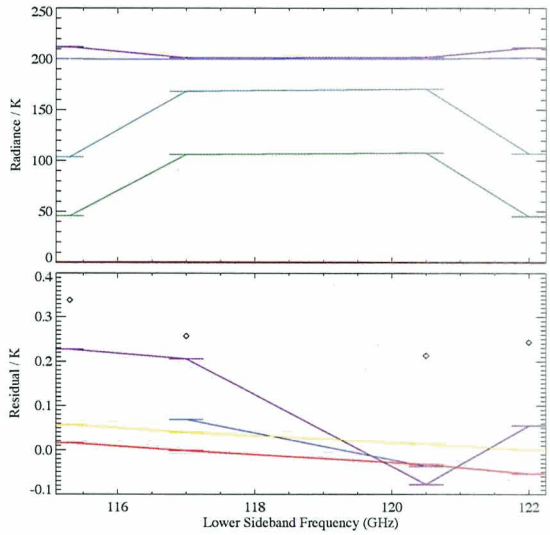

Figure 5. As in Figure 4, except for Band 32. Each of these Band-32 channels is 500-MHz wide, and they are on the wings of the 118-GHz O_2 line, outside of the Band 1 filterbank. Radiances are shown for six scan positions with approximate tangent altitudes: 3.5 km (purple), 11 km (blue), 18.4 km (dark green), 22 km (light green), 50 km (yellow), 87.9 km (red). Diamonds on the lower panel show theoretical precisions based upon radiometer noise and channel bandwidth, but these channel precisions are inflated to 1 K in χ^2 calculations of the retrieval to account for systematic uncertainties.

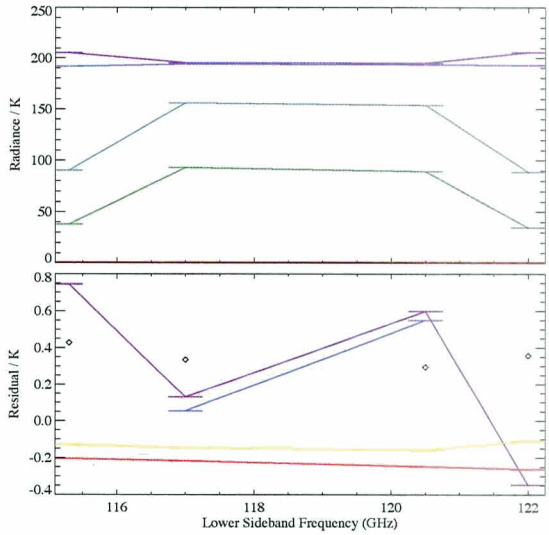

Figure 6. As for Figure 5, except for Band 34, which has the same channel positions for a second receiver (R1B) with the linear polarization orthogonal to that of Bands 1, 32, and 22. Again, data are global averages for 24 September, 2004.

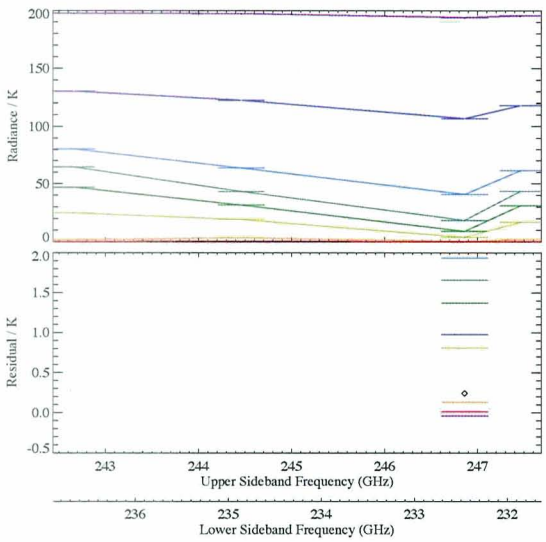

Figure 7. Top and bottom panels are as in Figure 4, except for Band 33. Data are global averages for 24 September, 2004. Channel 3 of Band 33 is a window channel with sidebands at 232 GHz and 247 GHz. Radiances are shown for eight scan positions with approximate tangent altitudes: 7.3 km (purple), 11 km (dark blue), 14.7 km (light blue), 18.4 km (dark green), 22 km (green), 26 km (yellow green), 35 km (orange), 45.5 km (red). Its radiance precision is inflated to 1 K in v2.2 retrievals to account for systematic uncertainties.

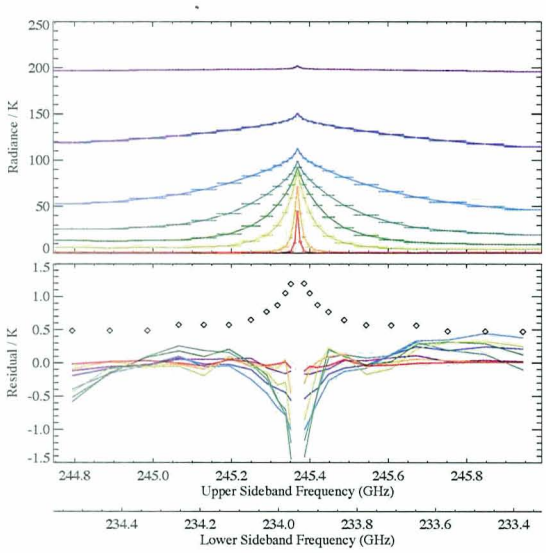

Figure 8. As in Figure 4, except for Band 8. Radiances are global averages from 24 September, 2004 for eight scan positions with approximate tangent altitudes: 7.3 km (purple), 11 km (dark blue), 14.7 km (light blue), 18.4 km (dark green), 22 km (green), 26 km (yellow green), 35 km (orange), 45.5 km (red).

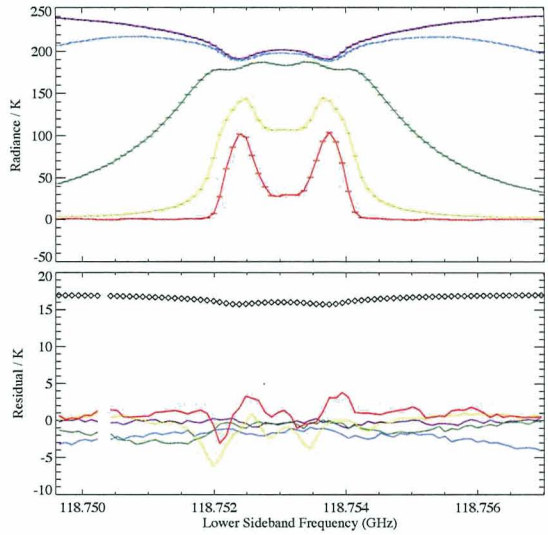

Figure 9. Top and bottom panels are as in Figure 4. Band 22 radiances cover the opaque line center of the 118.75 GHz O_2 line, which is Zeeman-split by the Earth's magnetic field. Radiances are shown for five scan positions with approximate tangent altitudes: 20 km (purple), 60 km (blue), 71 km (green), 81 km (yellow), 93 km (red).

above, have residuals of magnitude 0–1 K, with more variability among channels than is seen in the saturated radiances. Residuals in the unsaturated outer channels have an asymmetry about the line center which is not understood.

Bands 32 and 34, which have the same 500-MHz wide channels for horizontal and vertical linear polarizations, respectively, provide temperature information in the lowermost stratosphere and tropical tropopause layer. They have systematic residuals that are large compared to the retrieval's estimated measurement precisions. Polarization does not have a significant impact on these radiances, which are more than 1 GHz from the polarization-dependent, Zeeman-split O_2 line center, and signals should be approximately symmetric above and below the line center, so the set of four inner channels and the set of four outer channels should each be essentially quadruply redundant. The observed large residuals, which approach 1 K for the lowest-altitude views of band 34, are believed to be hardware-related, rather than the result of deficiency in geophysical modeling of radiances. The precisions of these channels have been inflated to 1 K so that the retrieval's χ 2 calculation does not force the retrieved state to closely fit these systematic errors.

Band 22 radiances and residuals are shown in Figure 9. Band 22 radiances cover the line center of the 118.75 GHz O_2 line, which is Zeeman-split by the Earth's magnetic field [*Schwartz et al.*, 2006]. The relative orientation of the Earth's magnetic field to the MLS R1A radiometer's field-of-view and polarization results in a pair of Zeeman

components being received by band 22 for most parts of an orbit. These radiances contribute to the temperature retrieval primarily in the mesosphere and lower thermosphere ($\sim$ 0.1 hPa–0.001 hPa.) The blue lines show radiances and residuals for a pointing with an average tangent height of $\sim$ 60 km ($\sim$0.22 hPa,) where the radiance is just starting to come out of saturation at the band edges. Residuals at this level are as large as 3–4 K in the band edges, and the inability of the retrieval to fit these radiances better may, in part, result from gain compression, which distorts spectral line shapes, as is discussed in Section 2.7. Unlike in the case of Band 1 radiances, band 22 radiances are used from where they are saturated to where they are optically thin. Residuals in the highest pointings shown ($\sim$ 81 km: yellow, $\sim$ 93 km: red) display a line-shift due to some combination of error in the Doppler-shift correction for spacecraft–earth relative motion and unmodeled mesospheric along-track wind, and provide an opportunity for along-track wind retrieval [e.g., *Limpasuvan et al.*, 2005].

2.6. Precision, scatter and spatial resolution

Each point in a retrieved MLS temperature of GPH profile is accompanied by an estimate of 'precision' taken from the diagonal elements of the solution covariance matrix [*Livesey et al.*, 2006] and mainly reflecting the contributions of radiance noise to the MLS measurements. Such estimates of precision are based upon the propagation of radiometric noise and of uncertainties in virtual measurements (such as the a priori temperature) through the measurement system. These values range from 0.6 K in the lower stratosphere to 2.5 K in the mesosphere and to 1 K at 316 hPa.

Precision can also be estimated from successive views of adequately similar scenes. As variability of the scene contributes something to the differences, analyses of these views provide an upper bound on precision values. Successive profiles generally see very similar scenes but have correlation due to shared calibration data, so their difference gives an unrealistically low value for precision. Profiles exactly one orbit apart are at the same latitude and local time, separated by 21 degrees of longitude. The RMS of differences between such pairs divided by the square-root of two provides an upper bound to the single-measurement precision. This estimate is best at latitudes and seasons where longitudinal variability is small and/or is a function only of local solar time. The smallest values found are from high-latitude summer, and are believed to be those least impacted by atmospheric variability. These values are slightly larger than those estimated by the measurement system in the troposphere and lower stratosphere and a factor of $\sim$ 1.4 larger from the middle stratosphere through the mesosphere.

Poleward of 70° S on February, 7, 2005, scatter in differences between successive orbits (divided by the square-root of two) is 1.5 K at 316 hPa, 1 K or less from 100 hPa to 10 hPa, 1.4 K at 1 hPa, 2.3 K at 0.1 hPa, 3 K at 0.01 hPa and 3.5 K at 0.001 hPa. Tropical orbital crossings from the same day (within 50 km in distance but 12-hours different in local time) have RMS differences of 1 K at 316 hPa, providing an even lower limit on precision at this level.

The 100-hPa level is the only GPH element included in the v2.2 state vector, so the diagonal matrix of the error covariance matrix only exists for this GPH level. GPH precision is calculated at other levels using the reference level precision and the profile of temperature precisions. Based upon this calculation, the 100-hPa reference level always has the minimum value in a GPH-precision profile, because precision at other levels is calculated by adding, in quadrature, the reference-level precision and the contribution of uncertain temperature in the GPH integrands. Properly calculated GPH uncertainty, using the full temperature/GPH error covariance matrix, would not necessarily have a minimum in precision at 100 hPa, but the 100 hPa level is, in fact, close to the level where line width information provides the best pointing/pressure reference. The impact of neglect of error correlation on calculated GPH values is expected to be less than 10 m. GPH precisions calculated using only the diagonal of the error covariance matrix are given in column 2 of Table 3. Values are $\sim$ 35 m from 316 hPa to 100 hPa, 44 m at 1 hPa, 110 m at 0.001 hPa.

The MLS retrieval algorithms operate in a two dimensional 'tomographic' manner [*Livesey and Read*, 2000; *Livesey et al.*, 2006]. This approach allows for the direct modeling of line-of-sight gradients. The resolution of the retrieved data can be describing using 'Averaging Kernels' [*Rodgers*, 2000]. The two-dimensional nature of the MLS retrieval system means that these kernels describe both vertical and horizontal resolution. Figure 10 shows horizontal and vertical averaging kernels for temperature. The vertical resolution of the MLS temperature measurement, as defined by the width of the kernels, is 5.3 km at 316 hPa,5 km at 100 hPa, 3.5 km at 32 hPa, 4 km at 10 hPa, 8 km at 1 hPa, 9 km at 0.1 hPa, 14 km at 0.01 hPa and 15 km at 0.001 hPa. In the along-track horizontal direction, the temperature data have single profile resolution ($\sim$165 km) through most of the profile, degrading to 185 km at 0.01 hPa and to 220 km at 0.001 hPa. The cross-track horizontal resolution is defined by the horizontal width of the MLS field of view. For the 240-GHz radiometer, which provides information in the troposphere, this is $\sim$6 km, and for the 118-GHz radiometer, which provides information from the tropopause upward, this is $\sim$ 12 km.

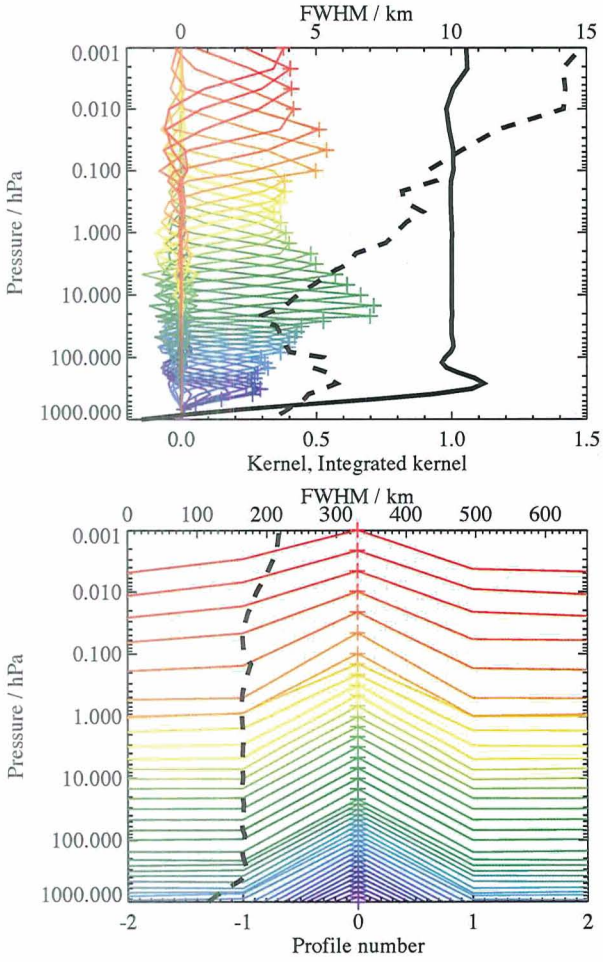

Figure 10. Typical two-dimensional (vertical and along-track horizontal) averaging kernels are shown for MLS v2.2 temperature at 35° N and in September; variation of these averaging kernels with latitude and season is small enough that these are representative for all profiles. Top: the vertical form of the averaging kernels (horizontally integrated). Individual colored lines show a the contribution of atmospheric temperatures at each level to a given MLS retrieved temperature, with the retrieval level marked by a + sign of the same color. The width of these functions is a measure of the vertical resolution of the MLS data. The full width at half maximum (approximately converted into kilometers) is shown by the thick black dashed line. The solid black line shows the integrated area under the kernels as a function of MLS retrieval level. Where the integrated area is close to unity, the majority of the information comes from the atmosphere. Lower values are associated with increased contributions from a priori information. Bottom: a similar plot indicating the horizontal form of the kernels. The colored lines show the horizontal kernel for a given height, with a decade of change in pressure used to denote a value of unity. Lines are offset so that their peak value is at the level indicated. The dashed black line is the full width at half maximum, in units of the MLS profile spacing (1.5° great circle angle ≈ 165 km).

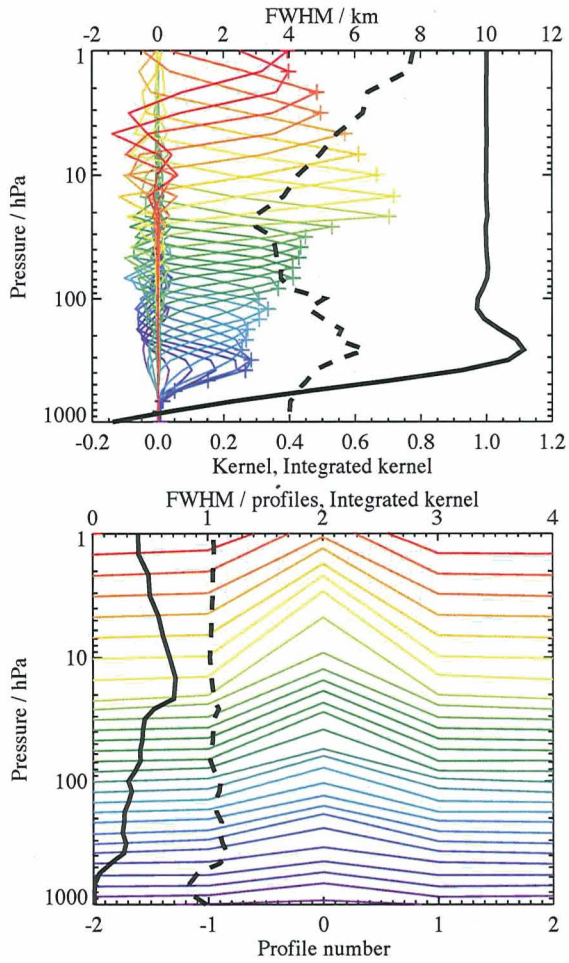

Figure 11. As Figure 10 but zoomed in on the stratosphere and troposphere.

2.7. Accuracy and Systematic Error Budgets

Quantification of various sources of systematic uncertainty is a major component of the MLS data validation. Systematic uncertainties arise from instrumental issues (e.g., radiometric calibration, field of view characterization), spectroscopic uncertainty, and approximations in the retrieval formulation and implementation. This section summarizes the relevant results of a comprehensive quantification of these uncertainties that was performed for all MLS products. More information on this assessment is given in Appendix A of *Read et al.* [2007a, this issue].

The impact on MLS measurements of radiance (or pointing where appropriate) of each identified source of systematic uncertainty has been quantified and modeled. These modeled impacts correspond to either 2-σ estimates of uncertainties in the relevant parameters, or an estimate of their maximum reasonable errors based on instrument knowledge and/or design requirements. The effect of these perturbations on retrieved MLS products has been quantified for each source of uncertainty by one of two methods.

The first method uses simulated MLS radiances generated from a day's observation of a model atmosphere. Sets of simulated radiances are generated, each with a 2-σ perturbation of some model parameter, and results of retrievals run on these radiances are differenced from retrievals run on unperturbed radiances. The impact of the perturbations varies from product to product and among uncertainty sources. Although the term 'systematic uncertainty' is often associated with consistent additive and/or multiplicative biases, many sources of 'systematic' uncertainty in the MLS measurement system give rise to additional scatter in the products. For example, although an error in the O_3 spectroscopy is a bias on the fundamental parameter, it has an effect on the retrievals of species with weaker signals (e.g., HNO_3) that is dependent on the amount and morphology of atmospheric ozone. The extent to which such terms can be expected to average down is estimated to first order by these 'full up studies' through their separate consideration of the bias and scatter each source of uncertainty introduces into the data. The difference between the retrieved product in the unperturbed run and the original 'truth' model atmosphere is taken as a measure of uncertainties due to retrieval formulation and numerics. Another retrieval of the unperturbed radiances is performed with 3 K added to the temperature a priori to test sensitivity to its value.

In the second method, the potential impact of some remaining (typically small) systematic uncertainties has been quantified through calculations based on simplified models of the MLS measurement system *Read et al.* [see 2007a, this issue]. Unlike the 'full up studies', these calculations only provide estimates of 'gain uncertainty' (i.e., possible multiplicative error) introduced by the source in question; this approach does not quantify possible biases or additional scatter for these minor sources of uncertainty.

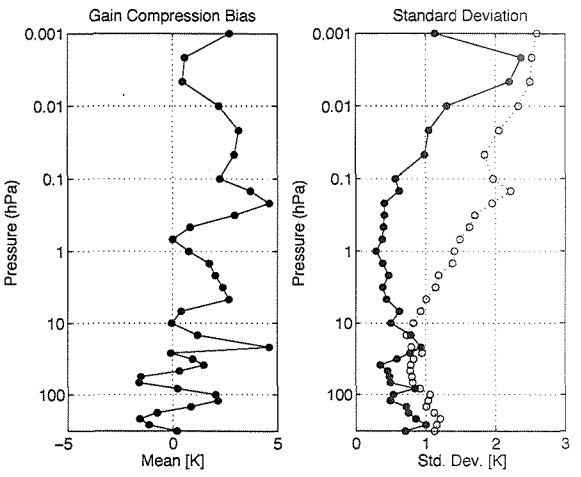

Figure 13. The modeled contribution of gain compression to systematic temperature error. Gain compression distorts spectral features, making temperature inferred from line-width-based pressure measurements and hydrostatic balance inconsistent with those made from saturated radiances. The left panel shows the mean difference between profiles retrieved from simulated radiances with and without gain compression. The right panel closed circles are the RMS scatter in the difference between the two retrievals. Open circles are the precision of the single-profile difference.

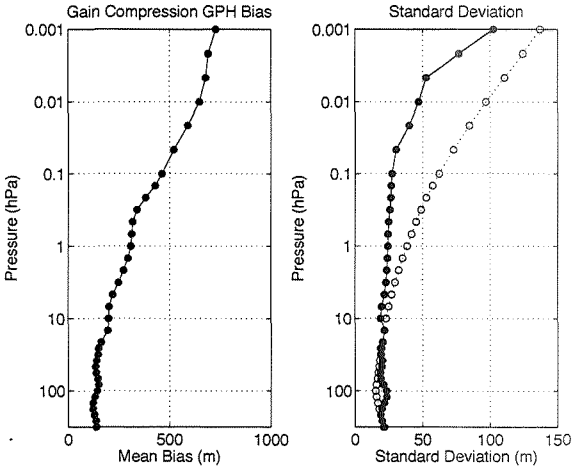

Figure 15. The modeled systematic error in GPH due to "gain compression." Panels are as in Figure /reffig:GainCompressionTBias. Gain Compression has the largest magnitude contribution to systematic error of any effect considered, and, unlike the others shown in Figure 14, the sign of this bias is significant. A retrieval run on simulated radiances with modeled gain compression matching best current estimates has a high bias in GPH at 100 hPa of $\sim$ 140 m compared to the control run, which is similar to the observed bias between MLS and GEOS-5 GPH.

Figures 12, 13, 14 and 15 summarize the results of this quantification for temperature and GPH. These show the magnitudes of expected biases and additional scatter the var-

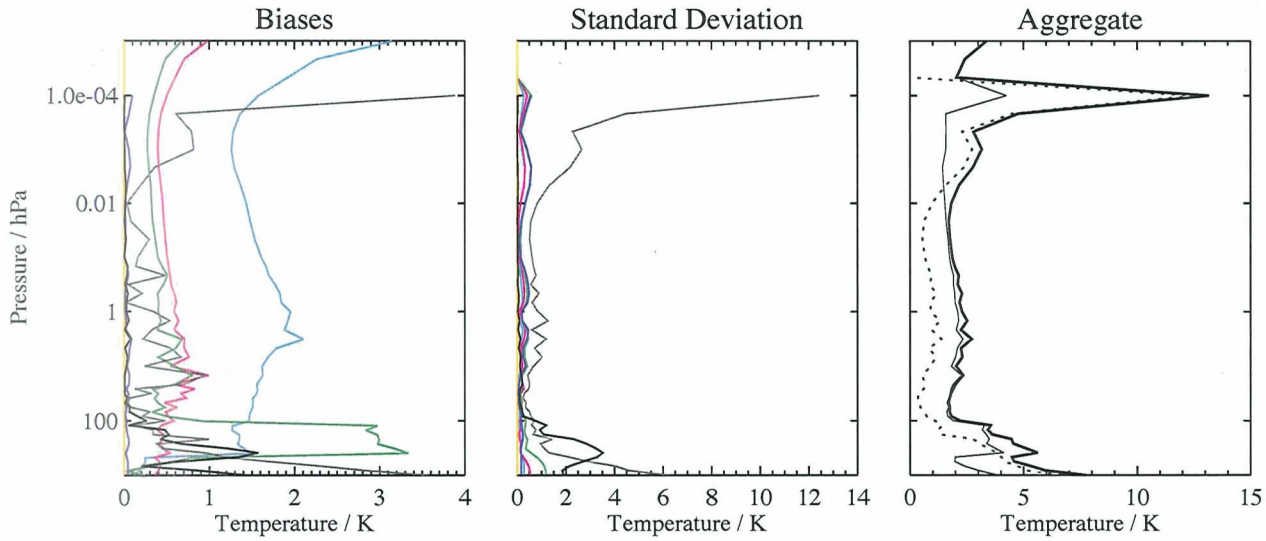

Figure 12. The estimated impact of various families of systematic uncertainties on the MLS temperature observations. The first two panels show the (left) magnitude of possible biases and (center) additional scatter introduced by the various families of errors, with each family denoted by a different colored line. Cyan lines denote errors in MLS radiometric and spectral calibration. Magenta lines show errors associated with the MLS field of view and antenna transmission efficiency. Red lines depict errors associated with MLS pointing uncertainty. The impact of possible errors in spectroscopic databases and forward model approximations are denoted by the green line, and the combined effect of error in retrieval numerics and sensitivity to a priori is shown in Grey. The blue lines show the impact of similar 'knock on' errors in other species. Finally, the typical impact of cloud contamination is denoted by the purple line. (Right) the root sum squares (RSS) of all the possible biases (thin solid line), all the additional scatters (thin dotted line), and the RSS sum of the two (thick solid line). Figure 13 show additional modeled systematic bias from "gain compression," for which a signed bias has been estimated.

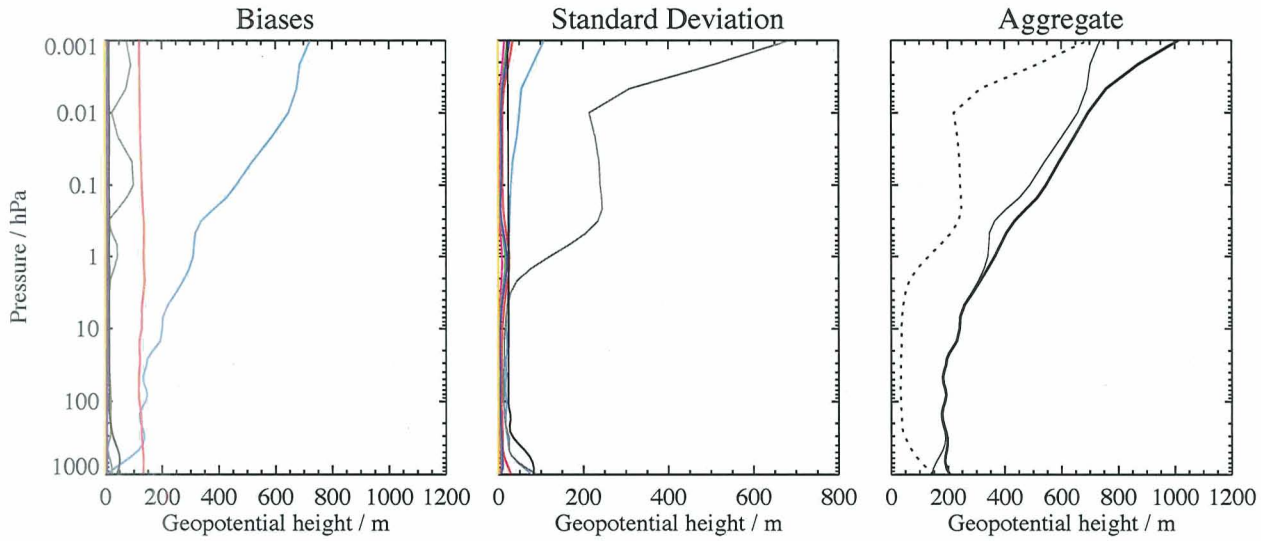

Figure 14. The estimated impact of various families of systematic errors on the MLS GPH observations. The description of the lines is the same as in Figure 12 for temperature.

ious errors may introduce into the data, and should be interpreted as 2-σ estimates of their likely magnitude.

The effects of "Gain Compression" are shown separately in Figures 13 and 15. Recent laboratory work by the MLS instrument team in estimating the impact of amplifier nonlinearity finds that observed spectrally-contrasting signals are "compressed" by $\sim$ 1.5 percent when viewed against a background scene of 300 K rather than against a scene close to 0 K. The magnitude of this distortion was not recognized until late in the development of version 2.2 algorithms, so there has been no attempt to correct for its impact on retrievals. Gain compression has the largest-magnitude contributions to systematic temperature and GPH bias of the suite of systematic uncertainty sources considered in this work. The other sources are modeled as random error in some parameter (e.g., radiometer pointing offset) propagated through the retrieval system, and the sign of the resulting error is unknown. For gain compression, both the sign of the bias and its magnitude are estimated. The impact of gain compression on retrieved temperature and on GPH are shown in Figures 13 and 15, respectively. Gain compression causes MLS v2.2 retrieved temperatures to have oscillatory vertical structure between 316 hPa and 10 hPa which is strikingly similar to that seen in comparisons with correlative data in Section 3. However, modeled gain compression also causes a 1–3 K high bias at levels above 10 hPa, while comparisons with correlative data generally suggest that MLS has a low bias at these levels. Thus, initial estimates are that correction for gain compression in a future version of the MLS retrieval will improve agreement with correlative measurements at lower retrieval levels but make it worse at higher levels.

Although the MLS observations are unaffected by thin cirrus clouds or stratospheric aerosols, thick clouds associated with deep convection can have an impact on the MLS radiances. The MLS Level 2 data processing algorithms discard or downplay radiances identified (through comparison with predictions from a clear-sky model) as being strongly affected by clouds [*Livesey et al.*, 2007b]. The contribution of cloud effects to the systematic uncertainty, both from the presence of clouds not thick enough to be screened out by the cloud filtering and from the loss of information through omission of cloud-impacted radiances, has been quantified by adding scattering from a representative cloud field to the simulated radiances and comparing retrievals based on these radiances to the unperturbed results. The cloud-induced effects on temperature shown in Figure 12 are estimated by considering only the cloudy profiles (as defined by the known amount of cloud in the 'truth' field). Cloud is estimated here to contribute 0.2 K or less to temperature bias at 100 hPa, increasing to $\sim$ 1.5 K with a $\sim$ 3.5 K standard deviation at 316 hPa. Cloud impacts are addressed further in Section 2.4.

The largest contributions to systematic temperature uncertainty, apart from 'gain compression, are from "radiometric/spectroscopic" sources and from those in the category "spectroscopy/forward model," shown in cyan and green, respectively, on Figure 12. The forward model contributes a bias uncertainty of $\sim$ 3 K in the upper troposphere where temperature information is primarily supplied by unsaturated radiances from the band 8, as discussed in Section 2.5. Uncertainty in the O_2 line width parameter results in systematic bias uncertainty of 0.5 K or less in the lower stratosphere and of 1 K or less in the troposphere. The contributions of antenna transmission and field-of-view shape uncertainties (the magenta line on Figure 12) are a $\sim$ 0.5 K systematic uncertainty bias which is nearly uniform with retrieval level. Their contribution to scatter is less than 0.3 K.

Over the range (316 hPa–0.001 hPa) of retrieval levels recommended for scientific use, this study indicates a bias uncertainty of up to 2–2.5 K between 100 hPa and 0.01 hPa, of up to 5 K at 316 hPa, and up to 3 K at 0.001 hPa. Additionally, gain compression contributes a generally positive bias to temperature between -2 K and 5 K with oscillatory vertical structure. The aggregate contribution to scatter is $\sim$ 1 K between 100 hPa and 0.01 hPa, increasing to $\sim$ 4 K between 100 hPa and 316 hPa and to $\sim$ 3 K between 0.01 hPa and 0.001 hPa.

Systematic uncertainty of GPH can be broken into uncertainties that affect GPH on the 100-hPa reference level, and those that affect GPH profiles through retrieved temperature uncertainties. The contribution of gain compression, shown in Figure 13, results in a positive bias of $\sim$ 140 m in the 100-hPa reference GPH as well as an increasingly positive bias with height. Other sources of systematic uncertainty contribute on the order of 150 m of bias of unknown sign. The largest terms are due to uncertainty in the O_2 line width ($\sim$ 100 m) and uncertainty in the 118-GHz radiometer field-of-view pointing offset from the 240-GHz radiometer ($\sim$ 100 m,) both of which are components of "pointing" on Figure 14. Retrieval numerics contribute up to 100 m of bias and up to 250 m of scatter in mesospheric GPH.

2.8. Comparison of v2.2 and v1.5 Temperature and GPH Data

This paper describes temperature and GPH produced by version 2.2 (v2.2) of the MLS data processing algorithms. The previous publicly release MLS data product, version 1.5 (v1.5) has been produced for the majority of days from August 2004 to the end of February 2007. Both v1.5 and v2.2 use radiances from MLS bands 22, 1, and 32/34, which are centered on the 118.75 GHz O_2 line, and are described in

Section 2.5. V2.2 also uses radiances from MLS band 8 and band 33 channel 3 near the isotopic $O^{18}O$ line at 236 GHz to improve resolution in the troposphere. V2.2 temperature, GPH and water vapor are retrieved on a higher-resolution grid in the troposphere and lower stratosphere, with 12 levels per decade from 1000 – 22 hPa rather than the 6-levels per decade of v1.5.

The MLS v2.2 temperature retrieval uses GEOS-5 temperature (discussed in Section 3.1) as its a priori while v1.5 used GEOS-4. Differences between these two model/assimilation are discussed in *Pawson et al.* [2007, this issue]. Of note is a significant low bias in GEOS-4 relative to GEOS-5 in the middle/upper stratosphere.

Figure 16 shows the mean difference between MLS v2.2 and MLS v1.5 temperature profiles from the first 93 days selected for processing with v2.2 algorithms. V2.2 has a general $\sim$ 2.5-K cold bias relative to v1.5 throughout the stratosphere and mesosphere, with an additional $\pm$2 K of persistent vertical oscillation. The exclusion of unsaturated radiances in the center of Band 1 in v2.2 retrievals changes the net effect of gain compression (discussed in Section2.7) on retrieved temperature, and is believed to be the main cause of this bias between versions. Figure 17 shows MLS v2.2 minus GEOS-5 temperature and MLS v1.5 minus GEOS-5 temperature, restricted to levels from 316 hPa to 1 hPa.

Figure 18 shows the difference between v2.2 and v1.5 retrieved GPH, averaged for the same 93-day period. The offset in the 100-hPa reference GPH levels retrieved by the two versions is small (0 ± 40 m), but the cold bias in v2.2 relative to v1.5 temperature results in a GPH low bias in v2.2 relative to v1.5 that reaches -600 m at 0.01 hPa.

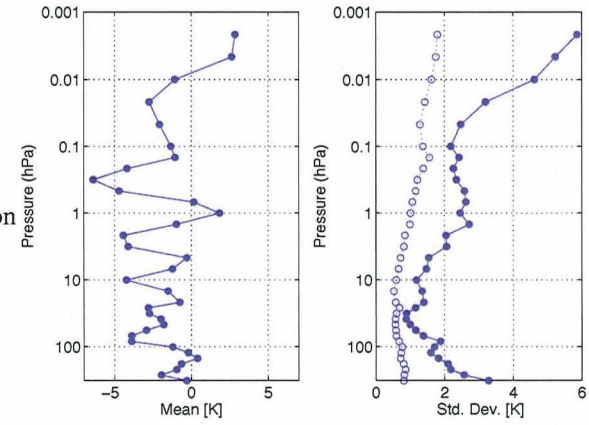

Figure 16. MLS v2.2 temperature minus v1.5 temperature, globally averaged for 93 days (287,000 profiles). The left panel shows the mean difference between v2.2 and v1.5. V2.2 has a general $\sim$ 2.5-K cold bias relative to v1.5 throughout the stratosphere and mesosphere, with an additional $\pm$2 K of vertical oscillation. Latitudinal variation (not shown) is small compared to persistent vertical structure shown. On the right panel, solid dots are the 1-σ scatter in individual pairs of profiles and open dots are the average combined estimated individual profile precisions from the two retrievals. MLS v1.5 has been linearly interpolated to the higher-resolution pressure grid of v2.2 in the UTLS.

3. Comparisons with Other Data Sources

In the following subsections, MLS temperature is compared to a number of correlative data sets. When comparing to gridded analyses (GEOS-5 and ECMWF), the analysis is interpolated in space and time to the location of MLS observations. A limited number of maps that have been produced from full resolution analysis will be so noted. In comparisons with profiles observed by other satellites or from radiosondes, "matched" pairs of profiles that are closely collocated in space and time are used. The coincidence criteria used to select the "matches" vary and are stated in each subsection below. A subsection comparing MLS temperature to radiosondes from the global radiosonde network has been omitted, as GEOS-5 and ECMWF analyses both assimilate the radiosonde measurements.

In making these comparisons, it is important to bear in mind that MLS data do not represent 'layer means', rather they define piecewise-linear profiles in log pressure that are

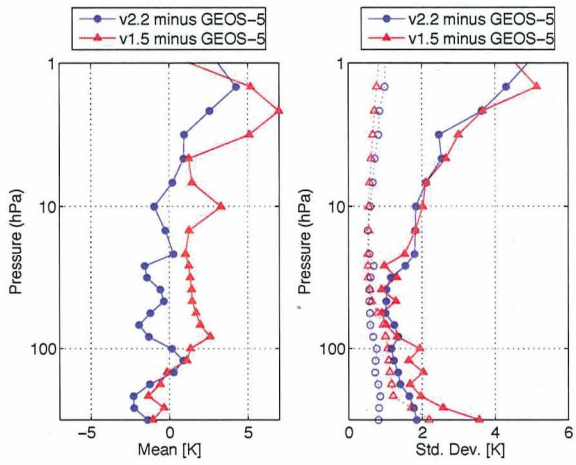

Figure 17. MLS v2.2 minus GEOS-5 temperature (blue circles) and MLS v1.5 minus GEOS-5 temperature(red triangles), globally averaged for 93 days (287,000 profiles). On the left panel, mean differences are shown and on the right panel, solid markers are 1 σ scatter about the means and open markers are the retrieval's average estimated single profile precisions.

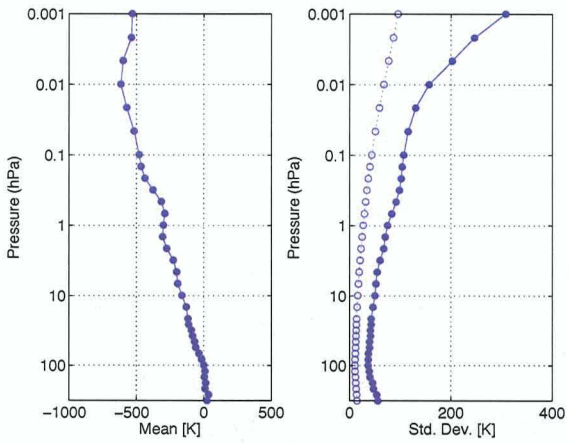

Figure 18. MLS v2.2 GPH minus MLS v1.5 GPH, averaged for the first 93 days of v2.2 processing. The panels are as in Figure 16. The two versions agree at 100 hPa to within a 1 σ scatter of 40 m, which reflects their use of the same pointing information. The relative temperature bias integrates into a negative bias of v2.2 relative to v1.5 that reaches 600 m at 0.01 hPa.

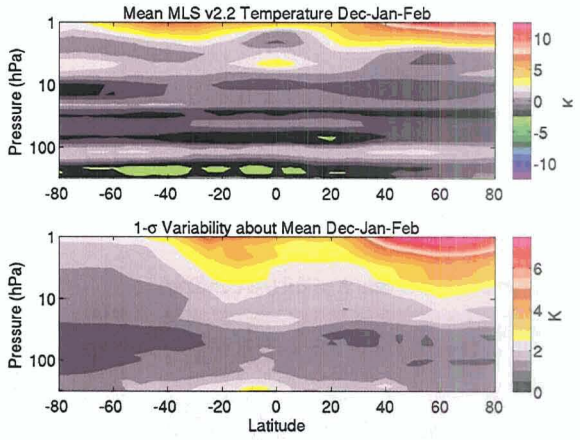

Figure 20. MLS minus GEOS-5 zonal mean temperature and variability averaged for December–February. A similar pattern, with north/south reversed, is seen in southern winter.

fitted to the observed radiances [*Read et al.*, 2006]. Accordingly, the most appropriate manner in which to compare MLS data to high vertical resolution correlative measurements is to find the piecewise linear fit of the MLS log-pressure grid that best fits the correlative data, and take its grid points [*Livesey et al.*, 2006]. This kind of piecewise linear representation might also be applied in the along-track direction, but its effect is negligible in temperature comparisons.

When evaluating the degree to which a high-vertical-resolution data set is consistent with MLS observations, convolution with MLS averaging kernels may also be needed. Fundamentally, the MLS measurement system retrieves differences from its a priori, which, for MLS v2.2 temperature, is GEOS-5 below 1 hPa and CIRA86 climatology above. When degrading a high-resolution correlative data set to check consistency with MLS observations, it is the difference between the correlative data set and a priori that is convolved with the MLS averaging kernels. Thus the MLS view of sharp features in a correlative data set's vertical temperature profile is degraded by its averaging kernel, but sharp features in the a priori may be passed into the MLS output state.

3.1. GEOS-5 Analysis

The GEOS-5 data assimilation system [*Rienecker et al.*, 2007] is a three-dimensional variational (3D-Var) system, combining observations in six-hour windows with six-hour general-circulation-model (GCM) forecasts. The incremental analysis update (IAU) approach [*Bloom et al.*, 1996] is used in the interface between the observations and the GCM to avoid shocking the model, thus producing smoother analyses. The GCM includes the finite-volume transport code of *Lin* [2004] along with a package of physical parameterizations. The configuration selected for this work was a 72-layer system with an upper level at 0.01 hPa; the layers transition from terrain-following coordinates in the lowermost troposphere to a pressure system near 186 hPa. A uniform horizontal grid of 0.66°-longitude by 0.5°-latitude was used. The assimilation is performed using the Gridpoint Statistical Interpolation (GSI) code of *Wu et al.* [2002]. GSI provides analyses for surface pressure, temperature, winds, moisture and ozone. Observations used to constrain the meteorology include the radiosonde network, infrared radiances from the High-Resolution Spectrometer (HIRS) and the Atmospheric Infrared Sounder (AIRS) on EOS-Aqua, and microwave radiances from the Advanced Microwave Sounding Units on NOAA-15 and NOAA-16; *Stajner et al.* [2007] describes screening and quality control for these observations.

Figure 19 shows MLS minus a priori (GEOS-5) data averaged for each of the 240 different 1.5° positions around an MLS orbit. MLS data are processed in 10-profile "chunks" plus some discarded overlap. Artifacts associated with chunk boundaries are apparent in the mean MLS minus GEOS-5 differences, particularly in the troposphere. At 261 hPa, these artifacts are as large as 1 K. Latitudinal variability is very similar between the hemispheres, and between the ascending and descending portions of the orbits. Vertically oscillating biases are on the order of 1–3 K, while latitudinal variability is typically 1 K. In the tropics at 147–68 hPa, MLS is cooler by ∼ 1 K compared to GEOS-5 than it is at higher latitudes. At 46 hPa and 38 hPa, the pattern is reversed, with ∼ 0.6-K positive biases in the tropics compared

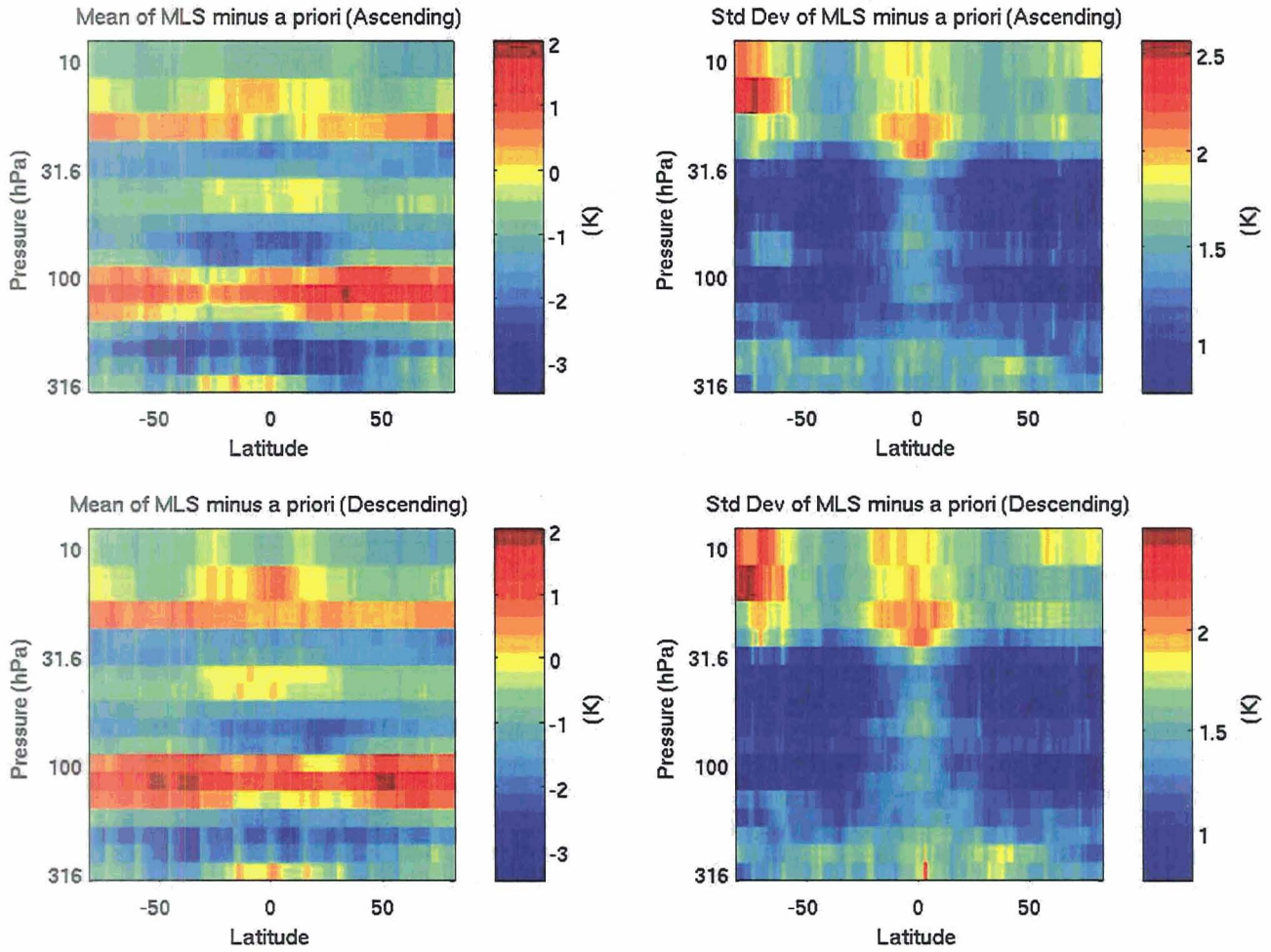

Figure 19. MLS minus a priori (GEOS-5) temperature and variability averaged by profile number in orbit, from 316 hPa to 10 hPa. Data are from 93 days processed with v2.2 algorithms and have been averaged for each of the 240 different 1.5° positions around an MLS orbit. The upper panels are the means and standard deviations from the ascending portion of the orbits and the lower panels are for the descending.

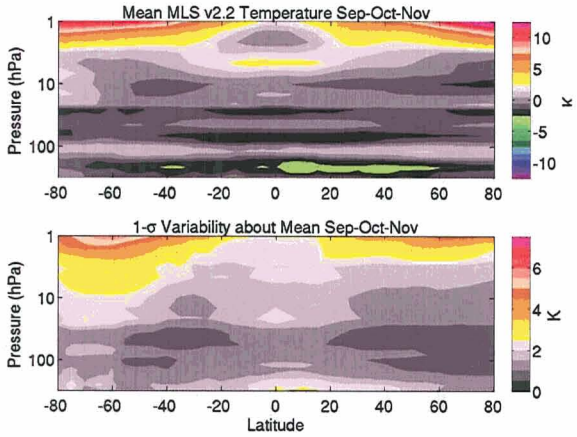

Figure 21. MLS minus GEOS-5 zonal mean temperature and variability averaged for September–November .

to those at higher latitudes.

Variability within these bins is shown in the right panels. The difference between MLS and GEOS-5 is $\sim$ 1 K in the lower stratosphere, increasing to $\sim$ 1.5 K in the troposphere. In the middle stratosphere, mid-latitudes have 1.5-K scatter while equatorial and polar bins have variability of 1.5–2.5 K.

Figure 22 shows the difference between MLS retrieved and a priori temperatures for January 28, 2005. The a priori temperature is GEOS-5 for levels below the 1 hPa surface and transitions over 5 km to CIRA86 climatology above. Selected levels from 316 hPa ($\sim$ 9 km) to 0.001 hPa ($\sim$ 91 km) are shown. Note, the scale on the y-axes is different in the different rows. Profiles that may have been influenced by cloud (non-zero Status) are shown in red. Those for which Quality was was less than 0.6 are shown in green. Outliers of as much as 10 K at the lowest recommended retrieval levels, 316–215 hPa, are believed to be due to the impact of clouds, as is discussed in Section 2.4.

Figure 20 and 21 show zonal mean curtain plots of the difference between MLS and GEOS-5 temperatures. On these plots, GEOS-5 does not transition to CIRA86 climatology as it does on plot showing a priori temperature. Colors in the upper plot are centered on 1-K intervals. Vertical oscillations between 316 hPa and 10 hPa are persistent, with peak-to-peak magnitude $\sim$ 4 K and latitudinal variation of $\sim$ 1 K. Northern winter (Figure 20) and southern winter (not shown) are similar. MLS is $\sim$ 10 K warmer than GEOS-5 at 1 hPa in the winter pole, and in both poles near equinox. Figure 23 shows seasonally-averaged, zonal-mean differences between MLS and a priori temperatures. In the upper troposphere and lower stratosphere (316 hPa – 10 hPa) where GEOS-5 is well supported by assimilated data, systematic biases are evident in the differences which are largely independent of

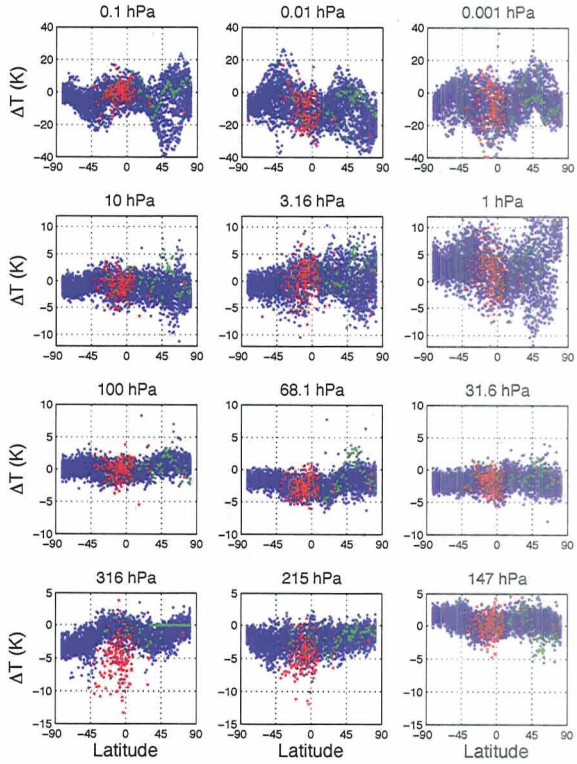

Figure 22. MLS v2.2 temperature minus retrieval a priori, for January 28, 2005. Green points have Quality < 0.6, and red points are flagged as possibly influenced by cloud using the method recommended in Section 2.3.

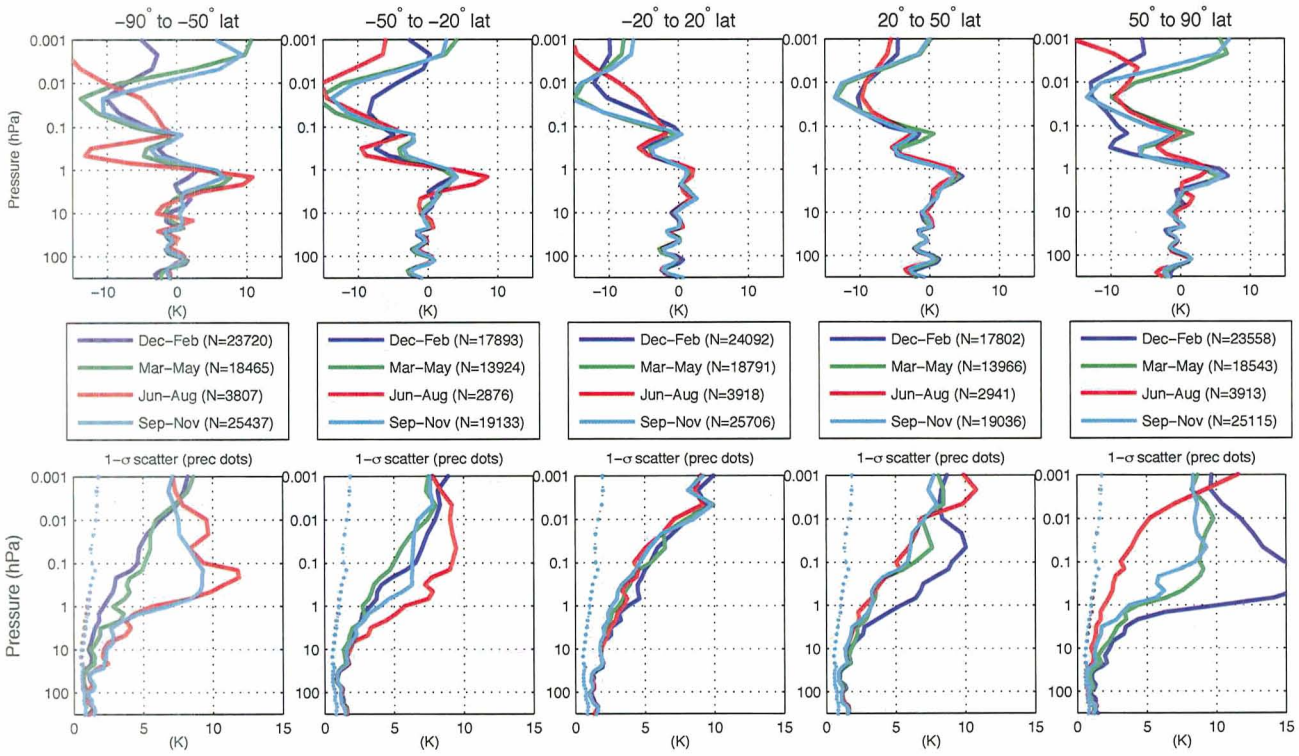

Figure 23. MLS v2.2 temperature minus its a priori. On this figure, and on several to follow, the upper panels are zonal mean differences with colored lines indicating seasons. The lower panels show the $1-\sigma$ scatter (standard deviation) about the mean. Dotted lines on the lower panel are estimated precision from the MLS retrieval. The values 'N' on the legends indicate the number of profiles that were averaged in each bin. Data are from 93 days selected for initial v2.2 processing from September 2004 – January 2007.

season and latitude. At pressures below 1 hPa, where a priori is CIRA86 climatology, mean differences exceed 10 K at some levels and seasons. Scatter in the differences, shown in the lower panels, exceeds 15 K in the northern winter polar mesosphere, where comparison is with climatology.

3.2. ECMWF Analysis

The European Center for Medium-Range Weather Forecast (ECMWF) assimilation is a 4D-Variational system based on a spectral GCM [e.g., *Simmons et al.*, 2005]. Operational ECMWF data used here are from two versions of the model. Prior to 1 February 2006, the operational data are from a T511/60-level model with a top at 60 km; after that time, the operational data are from a T799/91-level system with a top at 80 km. Further information on the high-resolution model is given by *Miller and Untch* [2005]. Changes to the ECMWF operational system are documented in the ECMWF newsletters, available at http://www.ecmwf.int/publications/newsletters/. Inputs to the ECMWF assimilation system are very similar to those listed for GEOS-5, including assimilation of AIRS radiances. Data from the T799/91-level model were made available beginning in October 2005, when a model experiment was running, but not operational. Model level data from the T799/91-level system are used at levels up to 0.1 hPa for profile comparisons. The T799/91-level data were extracted on a 2.5°×2.5°horizontal grid prior to interpolation to the MLS observation points. Figure 24 includes some ECMWF data interpolated to MLS locations from a 1°×1° grid and some from a 2.5°×2.5° grid. This difference in horizontal resolution of the grid on which data was extracted from the ECMWF analysis does not have a significant impact on the mean or scatters shown in the figure. Synoptic comparisons shown in sections 3.1 and 3.2 use the T511/60-level analyses after interpolation to a 0.5°×0.5° grid and to standard pressure levels.

Coincident profiles with MLS are constructed by interpolating the 6-hour ECMWF analyses in space and time to MLS observations. The vertical interpolation uses the least-squares fitting method, as discussed in the introduction to Section 3. Profiles have not been convolved with MLS averaging kernels. The vertical structure of the temperature biases, shown in the upper panels of Figure 24, has less than 1 K variability between seasonal and latitudinal bins from 316 hPa to 10 hPa. At these levels, the scatter between MLS and ECMWF (shown in the lower panels) is $\sim$ 1 K, which approaches MLS single measurement precision. In the upper stratosphere and mesosphere, the agreement between MLS and interpolated ECMWF becomes poorer and both biases and scatter have more seasonal and latitudinal variability. MLS has a low bias of -5 K to -12 K at 0.316 hPa. Winter high northern latitudes have scatter of 5–12 K between 1 hPa and 0.1 hPa.

3.3. CHAMP GPS Occultation

The CHAllenging Minisatellite Payload (CHAMP) [*Wickert et al.*, 2001] [*Hajj et al.*, 2004], launched into low-earth orbit in 2000, uses GPS radio occultation to obtain profiles of temperature. CHAMP retrieved temperatures between 10 and 35 km height have a mean bias of less than 0.4 K with respect to ECMWF analyses (a version which preceded the ECMWF T511 and T799 ECMWF analyses) and with respect to radiosonde data, and these differences have a height-dependent standard deviation of $\sim$ 1 K at 10 km and $\sim$ 2 K at 30 km [*Wickert et al.*, 2004]. The CHAMP retrieval solves for temperature from the top down until it reaches 250 K in the troposphere. At that point, water vapor contributions to GPS refractivity are no longer negligible.

CHAMP compares time delays as its line-of-sight to a GPS satellite passes through the atmospheric limb to time delays along paths just above the Earth atmosphere. It is considered to be "calibration-free" in the sense that the imprecision of its clock does not contribute significantly to the measurement error, nor does it drift appreciably over time. Intercomparison of temperature profiles from CHAMP and the similar SAC-C satellite are consistent to 0.05–0.1 K in mean and 0.5 K in standard deviation [*Hajj et al.*, 2004].

From the point of view of MLS intercomparisons in the upper troposphere and lower stratosphere (UTLS), CHAMP has the advantage that, unlike the radiosonde network or AIRS/AMSU, it is not assimilated into GEOS-5 or into ECMWF. CHAMP comparisons with MLS thus avoid any possible correlations that might be introduced through the use of GEOS-5 as the MLS a priori. This study uses 1525 MLS-CHAMP profile pairs coincident within 250 km and 3 hours from the period September, 2004 through October, 2006. The profiles are from 94 days which have been processed with MLS v2.2 algorithms.

Figure 25 shows global averages of MLS minus CHAMP, as well as MLS minus GEOS-5 and MLS minus ECMWF at the CHAMP coincidence points. In this figure, CHAMP has been fit to the MLS levels in the least-squares sense discussed at the beginning of Section 3, but it has not been convolved with the MLS averaging kernels. The mean biases between MLS and the other three data sets, shown in the left panel, agree to better than 1 K at most MLS retrieval levels between 316 hPa and 10 hPa. GEOS-5 and ECMWF are assimilating some of the same observations, but CHAMP is an independent observation of temperature. The common bias observed here is therefore likely to be a bias in the MLS measurement. The right panel shows the 1 σ scatter between the comparison pairs. The MLS-GEOS-5 and MLS-ECMWF

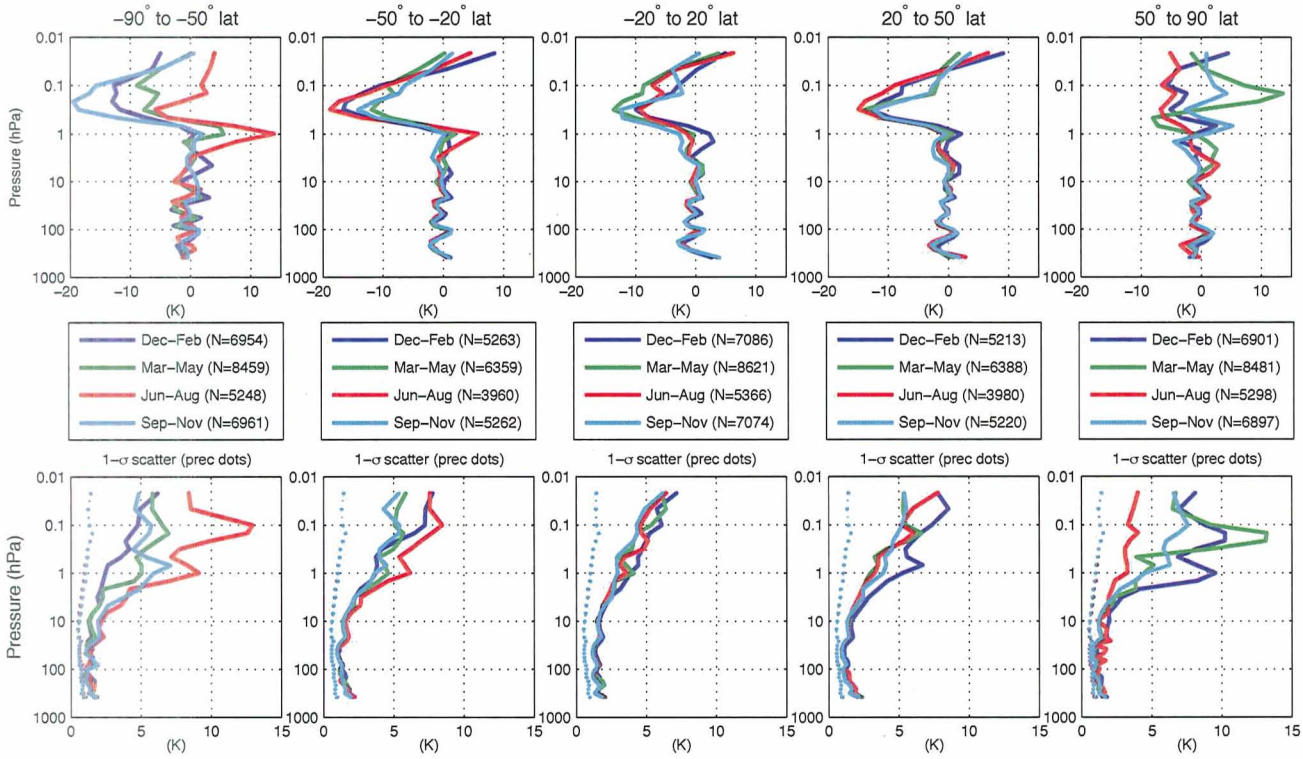

Figure 24. MLS v2.2 temperature minus interpolated ECMWF temperature are shown binned by latitude and season as in Figure 23. The dashed lines on the lower plot are typical MLS individual-profile precisions. Biases from 316 hPa to 1 hPa are similar for all latitudes and seasons. Individual-profile scatter about the mean biases in seasonal/latitudinal bins is ~ 1.5 K or less from 316 hPa to 10 hPa. These ECMWF data are from T799/91 only.

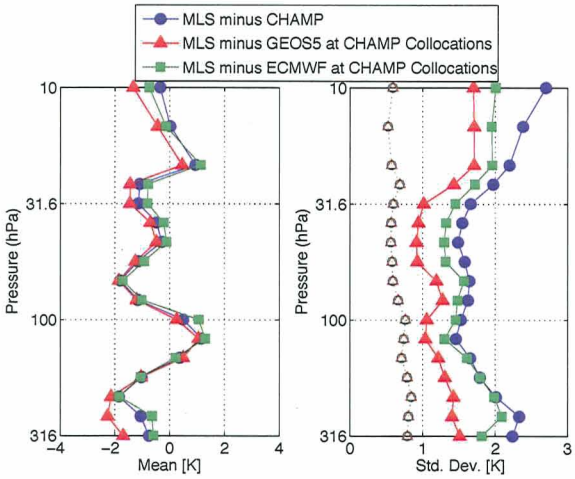

Figure 25. MLS v2.2 temperature minus CHAMP temperature, global average of 853 profiles. Open symbol on the right-hand plot are average MLS single-profile precision.

standard deviations are very similar, with the MLS-ECMWF line 0.2–0.3 K higher. MLS-CHAMP scatter is larger than that with GEOS-5 by $\sim$ 1 K from 14.7 hPa to 2.15 hPa. That scatter with the correlative data set (CHAMP) is not smaller than scatter with a priori is somewhat disappointing, but reflects both that CHAMP resolves vertical structure that MLS cannot, and the high degree to which GEOS-5 is a good representation of the atmosphere at these levels.

Figure 26 breaks out the MLS-minus-CHAMP collocations of Figure 25 by latitude and season, with mean MLS-minus-CHAMP differences (top row of panels) and standard deviation of the differences about the means (bottom row of panels.) Scatter in the summer high latitudes is $\sim$ 1 K between 100 hPa and 31.6 hPa, increasing to 2 K at 10 hPa and increasing to $\sim$ 2.5 K at 316 hPa. In the tropics, the scatter is 1.5–2 K from 316 hPa to 14.7 hPa, increasing above to 4 K at 3.16 hPa.

Figure 27 show scatter plots of selected levels. CHAMP minus GEOS-5 is on the x-axis and MLS minus GEOS-5 is on the y-axis. The separation of the outer black lines is twice the MLS estimated single-profile precision.

3.4. AIRS/AMSU

The Aqua satellite, which is in the same orbit as Aura, approximately 15 minutes ahead, carries three nadir-sounding instruments that have been used to produce a combined temperature product: the Atmospheric Infrared Sounder (AIRS) is a thermal-infrared grating spectrometer with 2378 spectral channels between 0.4 μm and 15.4 μm [*Pagano et al.*, 2003]; the Advanced Microwave Sounding Unit (AMSU) is a nadir microwave radiometer with 15 channels between 50 GHz

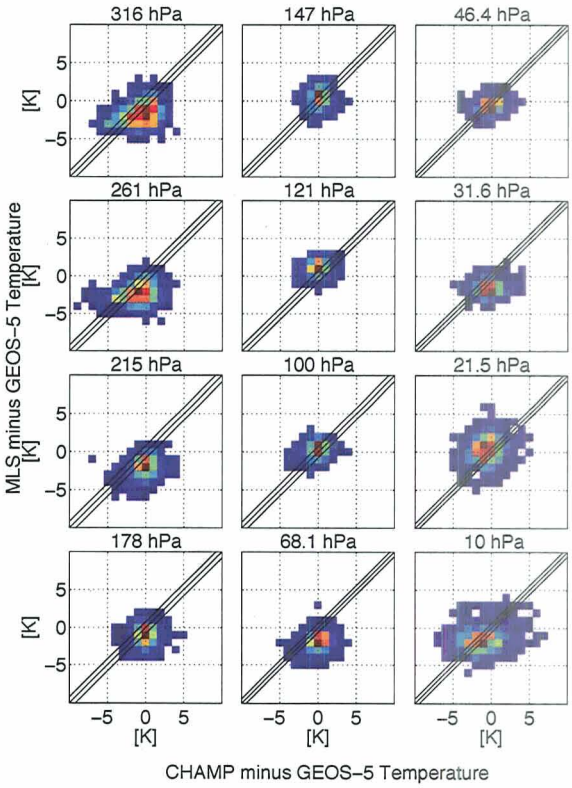

Figure 27. Scatter of MLS-minus-GEOS-5 and CHAMP-minus-GEOS-5 are shown. Colors are normalized to peak of distribution, with "hotter" colors indicating higher probability. The outer black lines are at plus and minus the MLS estimated precision (based upon radiance noise propagated through the measurement system) from the 1:1 line. Poor correlations indicate that MLS is generally not capturing much information in CHAMP that is not also in GEOS-5.

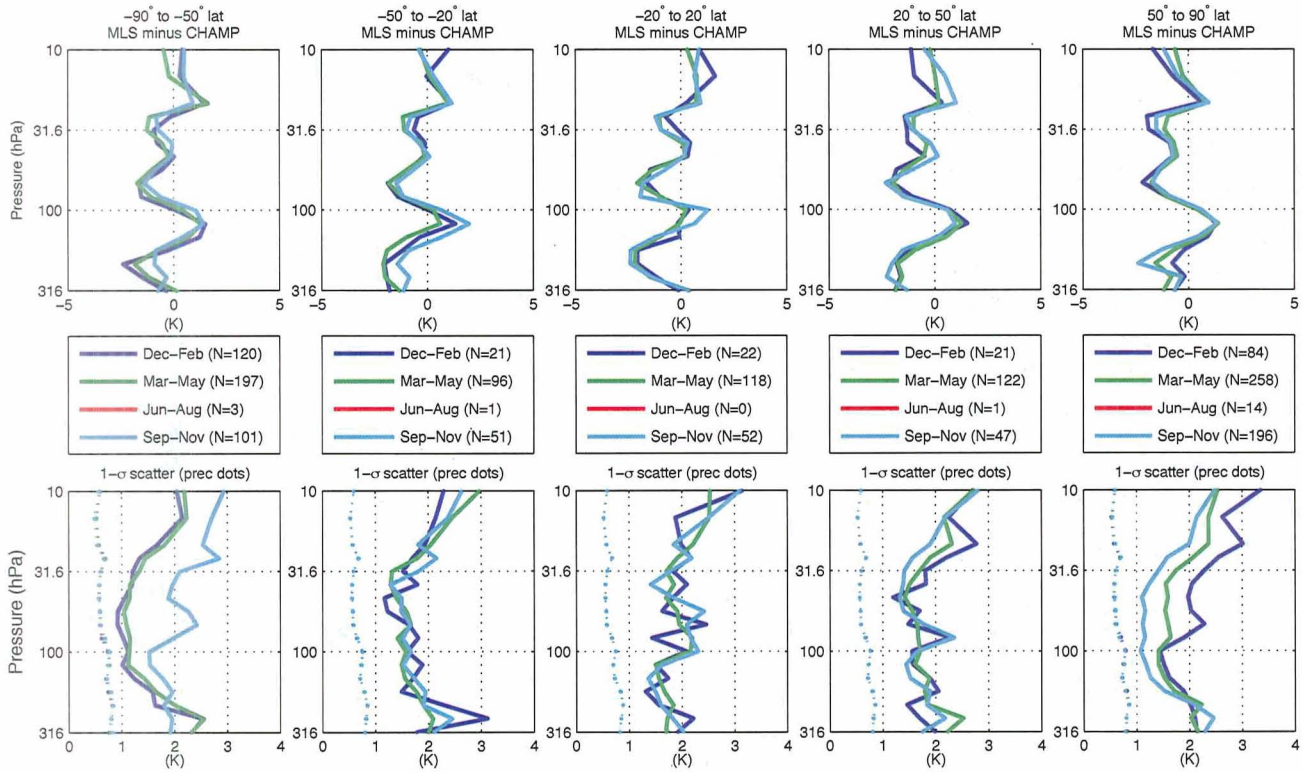

Figure 26. MLS v2.2 temperature minus CHAMP temperature, averaged in latitudinal and seasonal bins, as in Figure 23. The number of MLS profiles averaged, for each bin, is shown (N) in the center panel. Lower panels' solid lines are the 1-σ standard deviation of profiles about the mean profile of a given bin. Dotted lines are the average combined estimated precisions of a single MLS profile. The June–August lines have been removed because not enough coincidences have been found to give useful statistics.

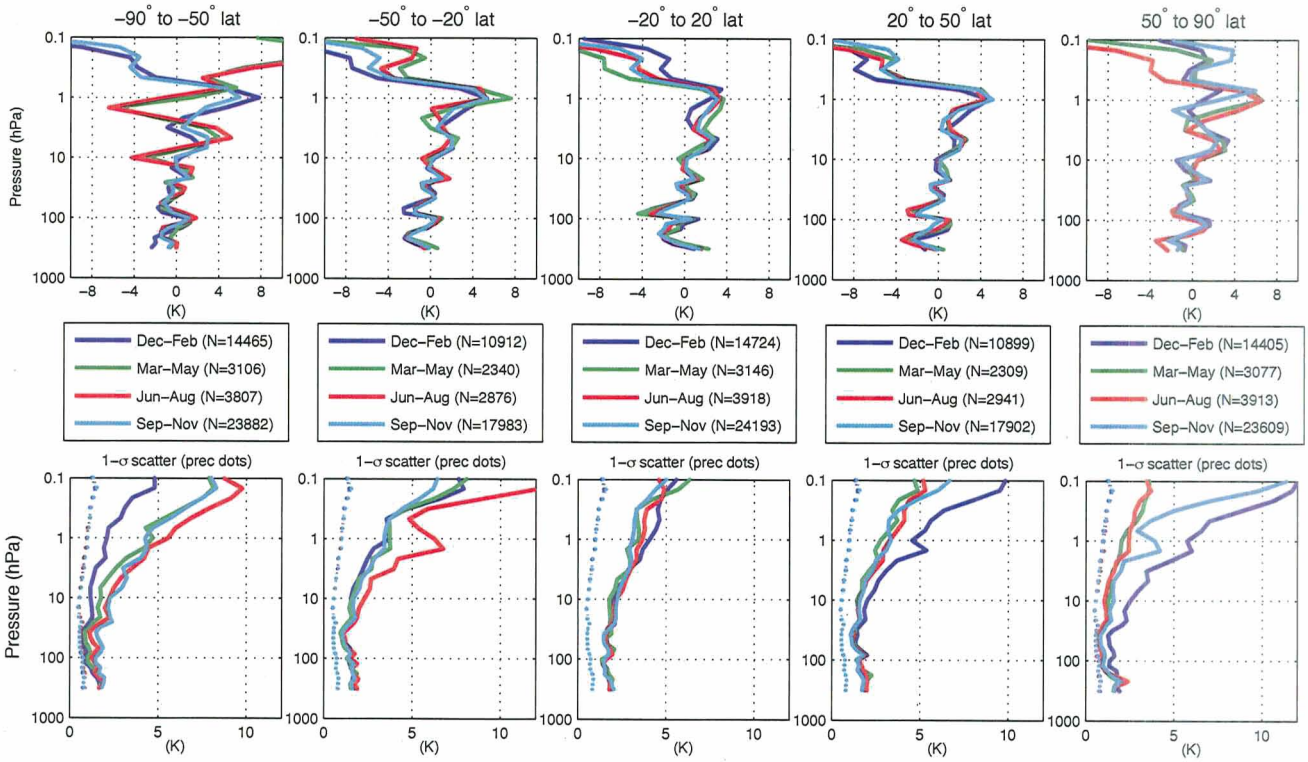

Figure 28. MLS v2.2 temperature minus AIRS/AMSU v4.0.9 temperature, averaged in latitudinal and seasonal bins, as in Figure 23. The number of MLS profiles averaged, for each bin, is shown (N) in the center panel. Lower panels' solid lines are the 1-σ standard deviation of profiles about the mean profile of a given bin. Dotted lines are the average combined estimated precisions of a single MLS profile and the AIRS/AMSU profiles to which it was compared.

and 90 GHz; a second microwave instrument, the Humidity Sounder for Brazil (HSB) failed prior to Aura launch [*Lambrigtsen*, 2003] in February 2003.

The AIRS/AMSU/HSB version 4 temperature product [*Chahine et al.*, 2006; *Susskind et al.*, 2003, 2006] has a nadir footprint approximately 50 km in diameter, commensurate with the AMSU field of view. The AIRS/AMSU temperature profiles shown by [*Divakarla et al.*, 2006] and [*Tobin et al.*, 2006] to agree with collocated radiosondes to within about 1 K in the troposphere and lower stratosphere. *Gettelman et al.* [2004] show similar agreement in the upper troposphere using aircraft observations. *Susskind et al.* [2006] show agreement to about 1 K up to the lower stratosphere in comparisons with European Center for Medium-range Weather Forecast (ECMWF) reanalyses. The ECMWF temperatures are strongly influenced by both operational radiosondes and operational AMSU instruments. The AIRS-ECMWF differences in *Susskind et al.* [2006] increase to 2.5 K at around 2 hPa. *Susskind et al.* [2003] demonstrate, through simulation, that AIRS vertical resolution is approximately 1 km. However, AIRS vertical resolution has not been established with AIRS retrieved profiles. The AIRS/AMSU observations include products compared with MLS retrievals in other studies. *Kahn et al.* [2007] examined cloud quantities, and *Read et al.* [2007b] and *Fetzer et al.* [2007] compare water vapor from the two instruments.

Through the first 2.5 years of the Aura mission, the MLS limb tangents have been well collocated with the center of the AIRS swath. Since MLS views forward along the orbital track at the atmospheric limb, MLS limb tangent points are only 7–8 minutes behind the AIRS nadir observations. In this study six AIRS/AMSU profiles, three on each side of nadir and closest in latitude to a given MLS profile, are averaged to give a profile collocated with MLS. AIRS temperature data are screened to remove the impact of clouds, as described in *Aumann et al.* [2005] and *Susskind et al.* [2006]. The resulting cloud-cleared, 150-km-along-track average by 100-km-across-track average AIRS temperature includes an MLS limb path that will come 8 minutes later.

MLS has biases with respect to AIRS/AMSU in the upper troposphere and lower stratosphere that are very similar to those that have been seen with respect to other correlative data sets. Figure 28 breaks out the biases and scatter into latitudinal and seasonal bins. Figure 36 (discussed later) shows a global comparison of MLS differences from correlative data sets. The oscillatory behavior between 10 hPa and 1 hPa for March–May and June–August in the 90° S–50° S latitude bin is also seen in SABER comparisons of Section 3.5, and warrants further investigation. At 0.1 hPa, AIRS/AMSU is $\sim$ 10 K warmer than MLS in most latitudinal-seasonal bins, and 5–10 K warmer than ACE, SABER and HALOE, discussed below.

3.5. SABER

The Sounding of the Atmosphere using Broadband Radiometry (SABER) [*Mlynczak and Russell*, 1995] instrument, launched on the Thermosphere Ionosphere Mesosphere Energetics and Dynamics (TIMED) satellite in December, 2001, measures profiles of kinetic temperature using 15-μm and 4.3-μm CO_2 limb-emission radiance measurements. Pressure is measured from spectral contrast and temperature is then inferred from pressure and pointing heights assuming hydrostatic equilibrium. The effective vertical resolution of SABER temperature is $\sim$ 2 km although it is retrieved on a higher-resolution fixed set of pressure surfaces [*Remsberg et al.*, 2003]. Version v1.06 SABER temperature, which is used in this study, has been extensively validated [*Remsberg et al.*, 2002, 2003].

Pairs of MLS and SABER profiles that are within 2 degrees of great circle arc (220 km) and 3 hours in time are compared. The first 72 days processed with v2.2 algorithms have 24,577 such coincidences. SABER retrieved values are provided at tangent points which sweep through a range of latitudes and longitudes, covering on the order of 300 km in a single profile. The SABER profile location in this study was taken from $\sim$ 0.1 hPa (SABER level number 246), which is near the mid-point of the profile. At the extreme ends of the profile, the distance between the SABER tangent point and the coincident MLS profile may be as much as $\sim$ 370 km. SABER data have been interpolated to MLS observation points using the least-squares method discussed in the introduction to Section 3, and then the portion that differs from the MLS a priori is convolved with MLS averaging kernels.

Non-thermodynamic equilibrium (non-LTE) effects in the very cold conditions ($\sim$ 130 K) of the summer polar mesopause (temperature minimum near 85 km) are not modeled in SABER v1.06, leading to a mesopause which is 3–5 km too low compared to climatological and falling spheres data [*Kutepov et al.*, 2006]. Version 1.07 of the SABER data corrects for non-LTE, lowering in altitude and warming the mesopause, but was not available at the time of this study. Non-LTE effects are not significant when temperature is above $\sim$170 K [*Mlynczak*, 2007].

Figure 29 shows global comparisons of coincident SABER and MLS profiles, with colors delineating season and columns latitude bins. As has been seen in comparisons with other data sets from 100–10 hPa, MLS has a similar cold bias with respect to SABER at all latitudes and seasons. The mean bias in this pressure decade is 2 to 3 K with an additional oscillation of $\sim$ 2 K peak-to-peak. The bias of -4 to -5 K at 261 hPa is larger in magnitude than is seen in comparisons with other data sets. Through most of the decade 10–

1 hPa MLS has a −1 K bias compared to SABER, however at 1 hPa, MLS has a 3 to 5 K high bias, and at 0.46–0.38 hPa a -3 to -5 K low bias.

In the summer polar mesosphere (red line on the 50° N–90° N panel and blue line on the 50° S–90° S panel) MLS has a large positive bias at 0.01 hPa (+12 K north, +7 K south) and a low bias at 0.001 hPa which is generally consistent with the anomalously low mesopause in v1.06 SABER data.

The 1-σ scatter (standard deviation) of MLS minus SABER from 100–10 hPa is $\sim$ 1 K in many of the latitude/seasonal bins, and is less than 1 K in the summer high latitudes. This scatter reflects the combined precision of MLS and SABER and variability from atmospheric gradients/imperfect coincidences; it may be taken as an upper bound on MLS precision at these levels. The larger variability observed in the winter poles results from differences between MLS and SABER sampling and the large temperature gradients associated with the winter polar vortices. In the decade 10–1 hPa the summer polar bins' scatter increases from 1–2.5 K and from 1–0.1 hPa increases from 2.5 K to 3 K. Other latitude/seasonal bins have scatter of 3–5 K in the 1–0.1 hPa decade except for southern summer bins, which are 5–7 K. From 0.1–0.001 hPa, scatter increases from $\sim$ 5 K to 12–15 K in all bins.

Figure 30 shows the global scatter of SABER temperature vs. MLS temperature at six representative levels. The very low ($\sim$ 150 K) temperatures of the summer polar mesosphere where non-LTE effects bias SABER temperatures are evident as outliers in the 0.01-hPa and 0.001-hPa bins. Figure 31 shows the scatter of SABER minus MLS a priori with MLS minus MLS a priori. Points where SABER temperature is less than 170 K have been removed. Global averages of the biases shown on Figure 29 for these six levels are evident as a 2 K low bias of MLS at 10 hPa, a 3–4 K high bias of MLS at 1 hPa and a 5–10 K low bias of MLS at 0.001 hPa. At 10 hPa there is some positive correlation, and at lower pressures, where CIRA climatology is the a priori, higher levels of correlation are evident. At 0.001 hPa,

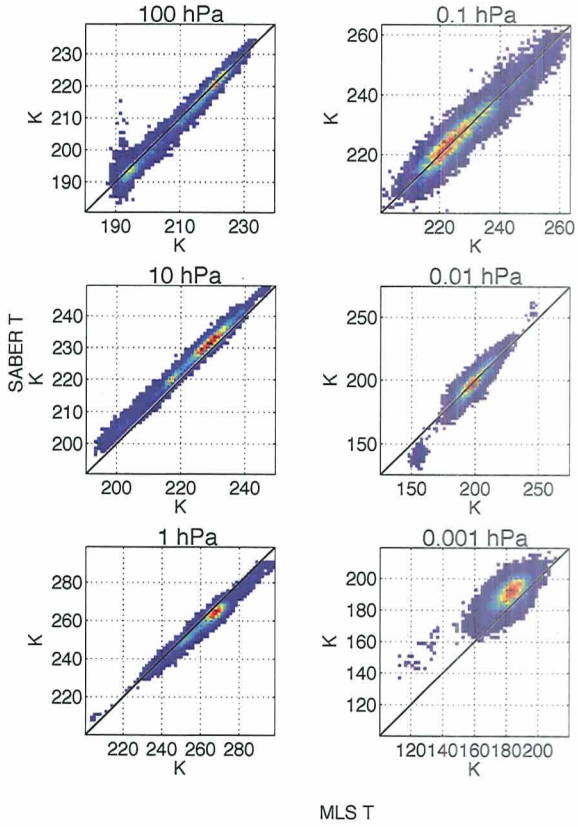

Figure 30. SABER temperature scattered against MLS temperature for six representative levels. The cluster of outlier points at 0.01 hPa near 150 K with a low SABER bias relative to MLS and those at 0.001 hPa with MLS temperatures 120–140 K and a high SABER bias relative to MLS are qualitatively consistent with the effects of non-LTE on SABER v1.06. These points are excluded in Figure 31.

3.6. HALOE

The Halogen Occultation Experiment (HALOE) on UARS measured profiles of limb path solar attenuation in eight infrared bands. These measurements are used to infer profiles of temperature, as well as gas mixing ratios of seven species and aerosol extinction. The HALOE temperature retrieval has been extensively validated [*Hervig et al.*, 1996; *Remsberg et al.*, 2002].

The HALOE V19 temperature is used in this study from 35 km to $\sim$ 85 km, where the signal-to-noise decreases to unity. At heights below 35 km altitude, aerosol significantly

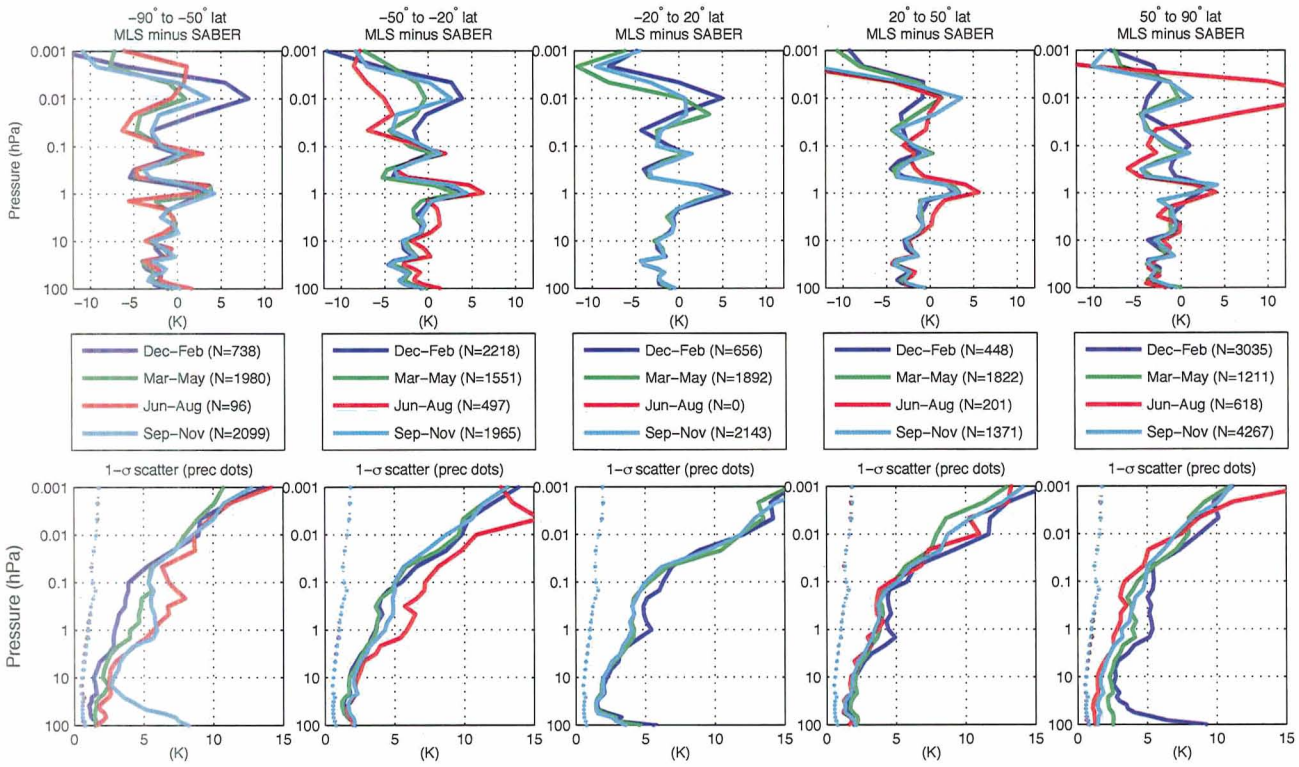

Figure 29. MLS v2.2 temperature minus SABER temperature, averaged in latitudinal and seasonal bins, as in Figure 23. The number of MLS profiles averaged, for each bin, is shown (N) in the center panel. Lower panels' solid lines are the 1-σ standard deviation of profiles about the mean profile of a given bin. Dotted lines are single-profile estimated precisions based upon propagated MLS radiometric noise.

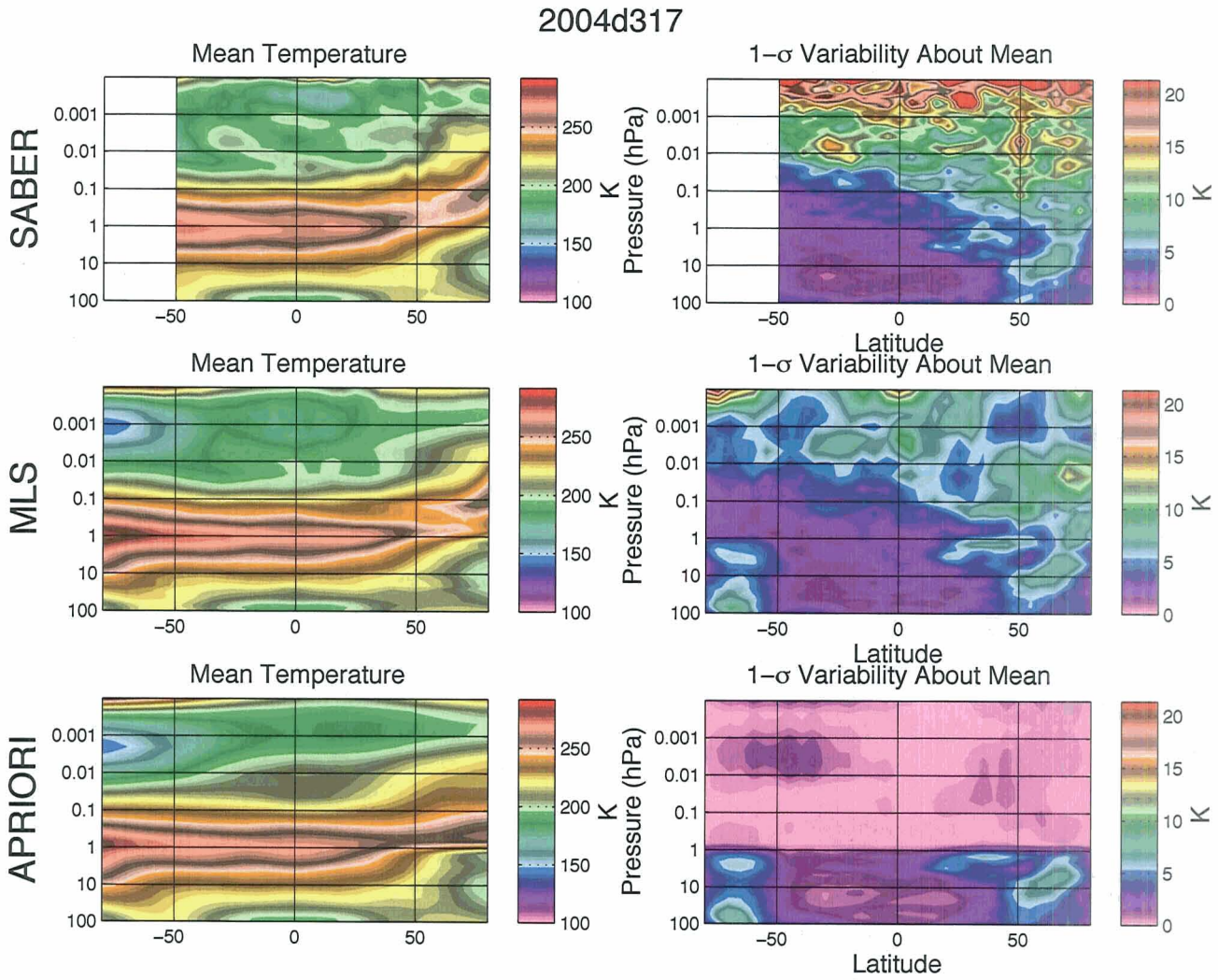

Figure 32. SABER descending, MLS ascending and MLS a priori temperature zonal means for November 12, 2004. MLS ascending and SABER descending branches are within 1.5 hours of local solar time from 20° S–70° N on this day. MLS a priori temperature is GEOS-5 at levels below 1 hPa and CIRA86 climatology above. SABER data has been interpolated to 12 levels-per-decade of pressure and has not been convolved with MLS averaging kernels. The color spacing on the left-hand, "zonal mean" plots is 3 K. MLS resolves something of the layered mesopause structure seen in SABER near 0.01 hPa, 30° S–equator, but nothing of the vertical structure at 0.001 hPa at the equator. Above the 0.1 hPa surface, MLS is on 3 levels-per-decade and its vertical resolution is 10 km or poorer. At these levels, SABER data which have not been degraded to MLS resolution have 1.5x–2x more zonal variability than does MLS.

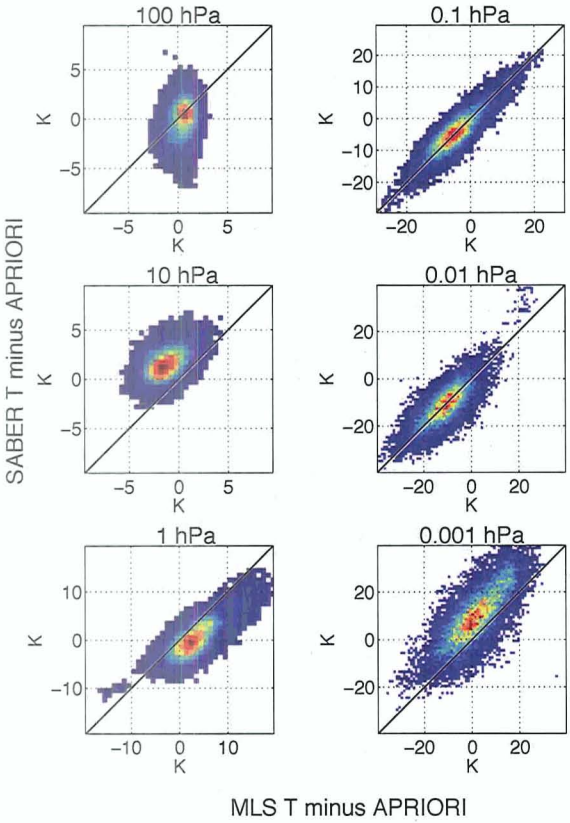

Figure 31. SABER temperature minus the MLS a priori is scattered against MLS temperature minus a priori. The MLS a priori is GEOS-5 below 1 hPa, CIRA climatology above 1 hPa and transitions between the two over 5-km around 1 hPa. This plot excludes pairs where either the MLS or SABER temperature is below 170 K to avoid non-LTE effects. The elongated distribution of SABER scatter relative to a priori at 100 hPa comes primarily from the December–February northern high latitudes and the September–November bin of the southern high latitudes, as seen in Figure 29.

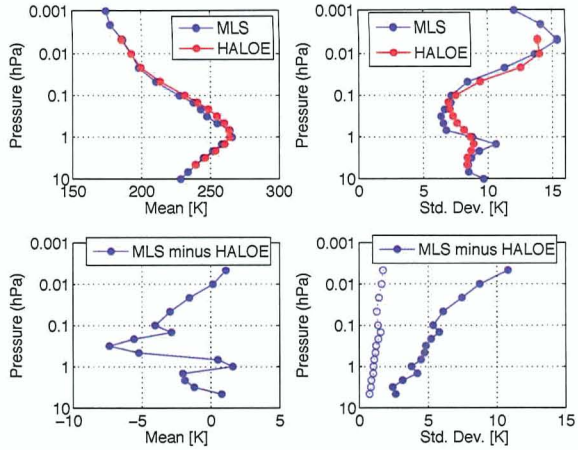

Figure 33. Globally averaged MLS v2.2 temperature minus HALOE V19 temperature. The upper panels show the means and standard deviations of collocated MLS and HALOE profiles. The lower panels show the mean and standard deviation of the difference.

impacts HALOE measurements, and the HALOE V19 files report NCEP temperature. Between 35 km and 45 km, the HALOE V19 transitions smoothly between NCEP temperature and temperature derived from occultation data. Typical measurement uncertainty, including random and systematic errors, is 5 K below 80 km [*Hervig et al.*, 1996; *Remsberg et al.*, 2002].

An improved HALOE product correcting for the effect of Polar Mesospheric Clouds (PMCs) was not available for this study. PMCs can cause high biases in V19 temperature of up to 10 K [*McHugh et al.*, 2003].

441 coincident HALOE profiles were found within 500 km and 6 hours of an MLS profile from September, 2004 through November, 2005. Several days with good latitudinal coverage in the MLS–HALOE coincidences were reprocessed with MLS v2.2. among the days prepared for the current suite of validation papers. No profile pairs are closer than 3 hours, and the mean absolute value of time difference is 4.4 hours.

Differences between collocated MLS and HALOE profiles are shown in Figure 33. The number of profiles is not sufficient to show latitudinal and seasonal variation. The coincidences shown are the closest MLS profile to a HALOE profile within 500 km and 6 hours. As a result of the 160 km along-track sampling of MLS, the "best" matched MLS profile is only very rarely more than 150 km away from its HALOE match in the meridional direction.

3.7. ACE-FTS

The Atmospheric Chemistry Experiment (ACE) was launched on the Canadian SCISAT-1 satellite on August 12, 2003[*Bernath*

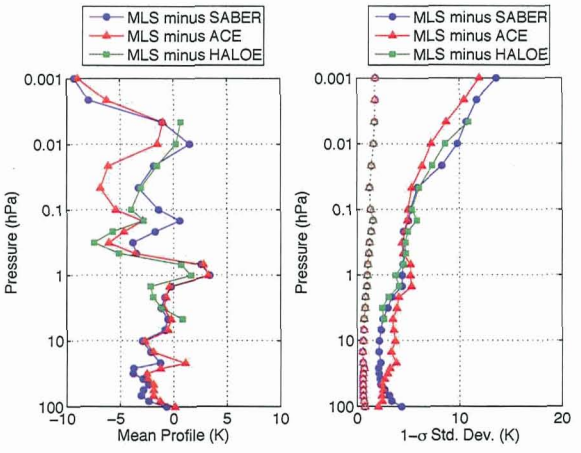

Figure 34. ACE minus MLS, SABER minus MLS and HALOE minus MLS, averaged for all coincident profiles. The left panel show mean biases and the right panel shows scatter about those means.

et al., 2004]. Its primary instrument is the ACE Fourier Transform Spectrometer (ACE-FTS), which will be referred to simply as ACE in this work, views sunrise and sunset occultations by the atmospheric limb with an infrared (2.2–13.3 μm) Fourier transform spectrometer that has 0.02 cm^{-1} spectral resolution. It is in a 74° inclination orbit that accumulates measurements of global coverage over one year, with extended periods viewing only at high latitudes. It has vertical resolution of $\sim$ 4 km. The ACE temperature retrieval process is described in detail in *Boone et al.* [2005]. Briefly, 106 spectral lines of CO2 between 930 and 3380 cm^{-1} are analyzed to determine pressure and temperature from the troposphere to the lower thermosphere. The current version of the ACE retrieval is 2.2. Initial validation studies using ACE version 1.0 have shown agreement between ACE and HALOE of $\pm$2 K [*McHugh et al.*, 2005], of better than $\pm$2.5 K with radiosondes from 10–30 km [*Kerzenmacher et al.*, 2005], and of better than $\pm$2.5 K with lidar measurements from 17–45 km [*Kerzenmacher et al.*, 2005].

894 MLS-ACE coincident profile pairs were identified in the first 93 days processed with MLS v2.2 algorithms. Coincidences were within 6 hours and within 10 degrees of longitude. MLS 1.5-degree along track sampling guarantees that the best coincident profiles match within 1 degree of latitude. Figure 34 shows mean biases (left) and standard deviations of differences (right) between MLS and ACE profiles, and also includes results for SABER and HALOE as a reference. MLS-ACE differences are consistent with MLS-HALOE and MLS-SABER differences to within 1.5 K in the stratosphere. ACE is 5–7 K warmer than MLS from 0.1 hPa to 0.02 hPa, and all three comparison data sets are 10 K warmer than MLS at 0.001 hPa.

3.8. Temperature Comparison Summary

The global mean bias of MLS temperature relative to eight correlative data sets is shown in Figure 35. Figure 36 is a magnified view of the lower portion of Figure 35. Between 316 hPa and 10 hPa, MLS has global biases with respect to ECMWF, GEOS-5, AIRS, radiosondes and CHAMP that agree to within $\sim$ 1 K. SABER, ACE and HALOE (which has valid data starting at 4.6 hPa) are generally warmer by 1–3 K in the stratosphere, but have similar vertical structure in their global biases with respect to MLS. Estimates of MLS systematic uncertainties are also shown. The black line is the predicted effect of amplifier gain compression base upon laboratory measurements of MLS flight-hardware-spare intermediate amplifiers and the gray shading about the black line is the 2-σ envelope of the combined systematic uncertainties discussed in Section 2.7. The gain-compression model explains most of the vertical structure of observed biases in the upper troposphere and stratosphere, although it predicts an unobserved $\sim$4-K bias at 21.5 hPa. In the mesosphere, the gain-compression model predicts that MLS would have a warm bias of 0–3 K, and other sources of systematic uncertainty are not large enough to explain the generally 0–7-K cold bias of MLS relative to SABER, ACE and HALOE.

Figure 37 shows representative temperature maps from MLS and SABER satellite data, and the GEOS-5, Met Office and ECMWF analyses, giving an overview of how these comparisons relate to representation of synoptic structure. The Met Office analyses are described briefly by *Manney et al.* [2007, this issue] and in detail by *Swinbank et al.* [2002, 2004]; *Davies et al.* [2005, and references therein]; the top analyses level for MetO is 0.1 hPa, lower than that for ECMWF T799/91-level and GEOS-5. In the middle and lower stratosphere, there is very good, detailed, agreement in the morphology of the temperature fields from both satellite instruments and the three analyses. SABER temperatures are generally slightly higher than those in the analyses, and thus MLS shows a larger low bias with respect to SABER. In all cases, the biases appear to be largely spatially uniform. In the upper stratosphere, where the analyses are poorly constrained by data, the three assimilated datasets show some qualitative differences, and quite large quantitative ones (e.g., the GEOS-5 analyses are quite cold with respect to Met Office and ECMWF); these differences arise largely from differences in the resolution, vertical range and gravity-wave drag in the GCMs underlying the three analyses [e.g. *Fritts and Alexander*, 2003]. MLS and SABER show largely good qualitative agreement, but with some differences in the warm pools at high latitudes; the positions of those warm pools in the satellite data agree better with GEOS-5 and ECMWF than with Met Office. MLS shows a

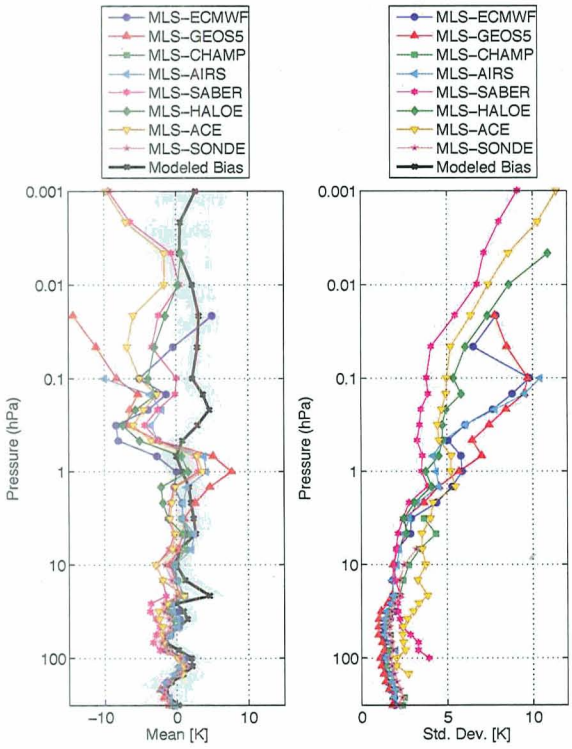

Figure 35. Summary of temperature biases and scatter between MLS and eight correlative data sets. Mean differences are shown in the left panel and scatter about these differences in the right. Figure 36 shows the same data, but limits pressures to 1 hPa or greater. Mean differences from 3.16 hPa to 0.1 hPa are correlated among the comparisons are likely indicate a bias in MLS measurements.

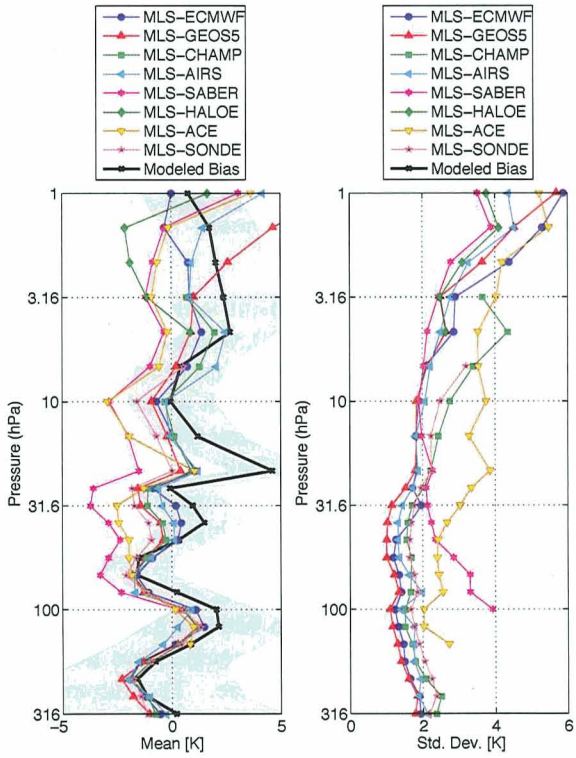

Figure 36. Global tropospheric and stratospheric temperature biases (left panel) and scatter of differences (right panel) between MLS and eight correlative data sets are shown. Modeled systematic uncertainties (discussed in Section 2.7) are also shown, with gain compression in black and the 2-σ contribution of the other terms, which are biases of unknown sign, summarized by the gray envelope. Mean differences are shown in the left panel and scatter about these differences in the right. Figure 35 shows the same data, with expanded vertical and temperature axis ranges. Mean differences from 3.16 hPa to 0.1 hPa are correlated among the comparisons are likely indicate a bias in MLS measurements.

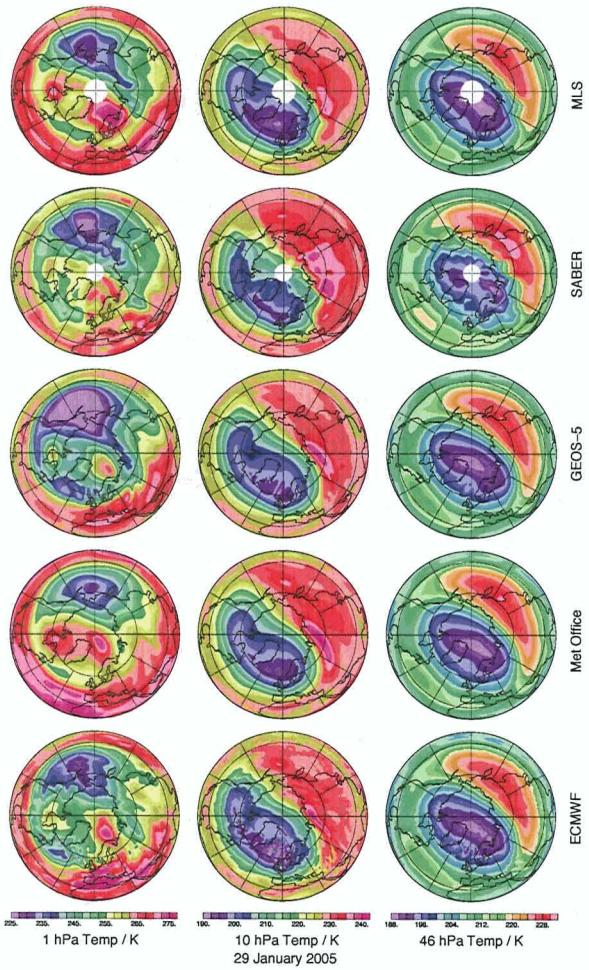

Figure 37. MLS, SABER, GEOS-5, Met Office and ECMWF northern polar daily temperature maps for 29 January, 2005 in the upper (left), middle (center), and lower (right) stratosphere. MLS and SABER data are gridded by taking a distance-weighted average around each gridpoint of all data taken in a 24-hour period centered at 12 UT; the MLS grid is 2°×5° and the SABER grid 4°×5°. GEOS-5, Met Office, and ECMWF (T512/L60) data are on 0.5°×0.66°, 2.5°×2.5°, and 0.5°×0.5° grids, respectively. Projection is orthographic, with 0° longitude at the bottom and 90°E to the right; latitude domain is 0° to 90°N.

small high bias with respect to SABER at 1 hPa; biases with respect to the analyses are more position-dependent than at lower levels, with, e.g., good agreement of minimum values with ECMWF but higher maximum values in high-latitude warm pools.

3.9. GPH Comparisons

MLS v2.2 100 hPa reference GPH (refGPH) is typically 100–250 m higher than GEOS-5 in the northern high latitudes and 50–200 m higher than GEOS-5 in the Southern high latitudes. At low latitudes, the ascending branch of the orbit is typically 0–120 m higher than GEOS-5 while the descending branch is 100-200 m higher. A seasonal cycle in the daily mean differences of ∼ 100 m peak-to-peak is evident in the high-southern latitudes (peaking in January) and in the ascending branch of the equatorial mean differences (peaking in July) There has been a general downward trend in the MLS minus GEOS-5 bias of 40–50 m/year over the life of the mission. Correction of gain compression, which is neglected in v02.20 retrievals, lowers MLS 100 hPa GPH by ∼ 150 m, bringing it into better agreement with GEOS-5. The gain-compression parameter (discussed in Section 2.7) has not been tuned to match observed temperature or GPH biases, but rather was measured in the laboratory using spare flight hardware. MLS v2.2 GPH has a bias of ∼ 100 m at 10 hPa with respect to GEOS-5 and SABER, and the bias with respect to SABER becomes increasingly negative at lower pressures: ∼ −100 m at 0.01 hPa and ∼ −500 m at 0.001 hPa. These negative biases reflect the general low temperature bias of MLS with respect to SABER.

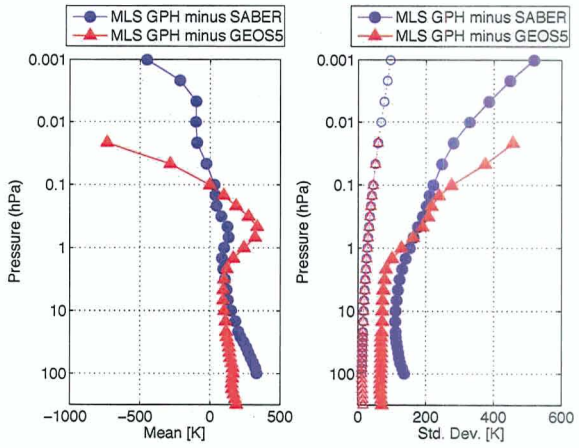

Figure 38. Globally-averaged MLS GPH minus SABER GPH (blue) and MLS GPH minus GEOS-5 GPH (red) averaged over the same profile pairs.

Figure 38 shows globally-averaged differences between MLS GPH and SABER GPH and between MLS GPH and GEOS-5 GPH. The slopes of the curves on the left-hand plot are proportional to the average temperature difference between the two data sets at a given level. In both cases, the increasingly large low bias of MLS GPH with height results from an overall low bias in MLS temperature relative to the correlative data sets. GEOS-5 is expected to be the more-reliable of these two correlative data sets in the troposphere and lower stratosphere, where it is well-supported by assimilated sondes and other measurements. In the mesosphere, SABER has good sensitivity and should be preferred to GEOS-5. In the upper stratosphere, there is generally good agreement between the two correlative data sets.

Figure 39 shows stratospheric maps of GPH for Jan-

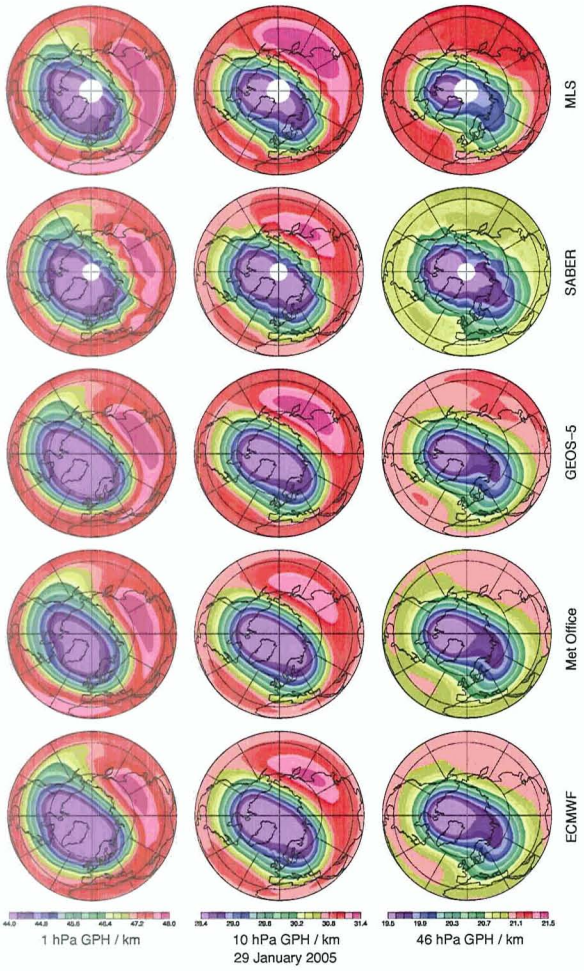

Figure 39. MLS, SABER, GEOS-5, Met Office and ECMWF northern polar stratospheric daily maps of GPH for 29 January, 2005. Layout is as in Figure 37.

uary 29, 2005 from MLS, SABER, GEOS-5, Met Office and ECMWF. Although the MLS GPH offset is apparent in the overall values, the morphology of the fields, including the vortex (low GPH) and anticyclone (high GPH) shapes and positions, and gradients surrounding the vortex, appear to agree very well at all levels with both SABER and the meteorological analyses. Figure 40 shows similar maps from MLS, SABER and GEOS-5 in the mesosphere. At these levels, there are no data inputs into the assimilation systems, so the only data influence on them is from effects that propagate from lower levels; thus the GEOS-5 analyses here are reflecting mainly the behavior of the underlying GCM, increasingly so at higher levels. Consistent with this, while the morphology of and gradients in MLS and SABER GPH agree quite well at all levels shown, qualitative agreement with GEOS-5 is seen only at 0.1 hPa.

GPH is often useful in studies of the synoptic circula-

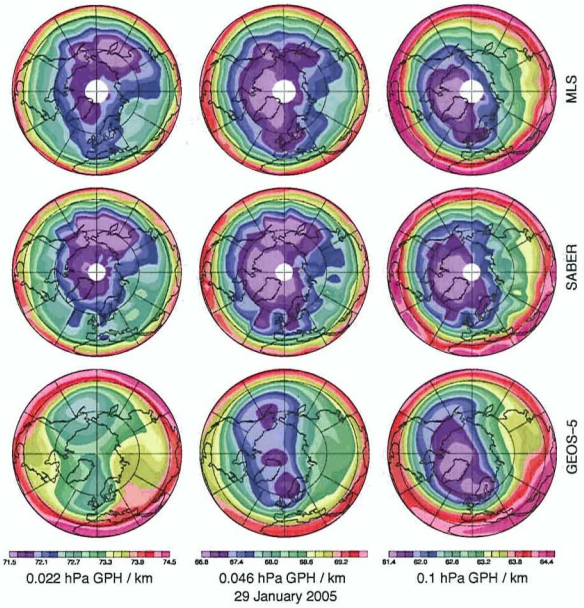

Figure 40. MLS, SABER, and GEOS-5 northern polar mesospheric daily maps of GPH for 29 January, 2005. Levels shown are 0.022 hPa (left), 0.046 hPa (center), and 0.1 hPa (right). Layout is as in Figure 37.

tion, especially wave motions and their time evolution and related diagnostics. Figure 41 compares the wave 1 amplitude in MLS GPH with SABER and GEOS-5 from the upper troposphere into the mesosphere on a day in the NH winter. Consistent with the maps shown above, in the upper troposphere through mid-stratosphere, where GEOS-5 analyses are well-constrained by data and the dynamics in the GCM well-known, MLS wave 1 structure and amplitude agree very well with GEOS-5; agreement between MLS and SABER in the lower part of this range, where SABER data quality is not as good, is not as close. Conversely, in the upper stratosphere and mesosphere, where SABER data quality is expected to be good and GEOS-5 is not constrained by data, MLS GPH agrees much more closely with SABER than with GEOS-5. In particular, both MLS and SABER capture the minimum in wave amplitude above the stratopause and increasing amplitude above that, which is nonexistent in GEOS-5. The failure of GEOS-5 to capture this may be related to the parameterization of gravity-wave breaking (which can strongly influence planetary-scale wave amplitudes at these levels [e.g. *McLandress and McFarlane*, 1993]) and/or other model deficiencies. Comparisons of the time evolution of planetary-scale waves in MLS, SABER and meteorological analyses (not shown) also indicate very good quantitative agreement in timing, magnitude and phase of variation. The availability of mesospheric GPH measurements from MLS and SABER, and the structural agreement between them (which gives confidence in their overall qual-

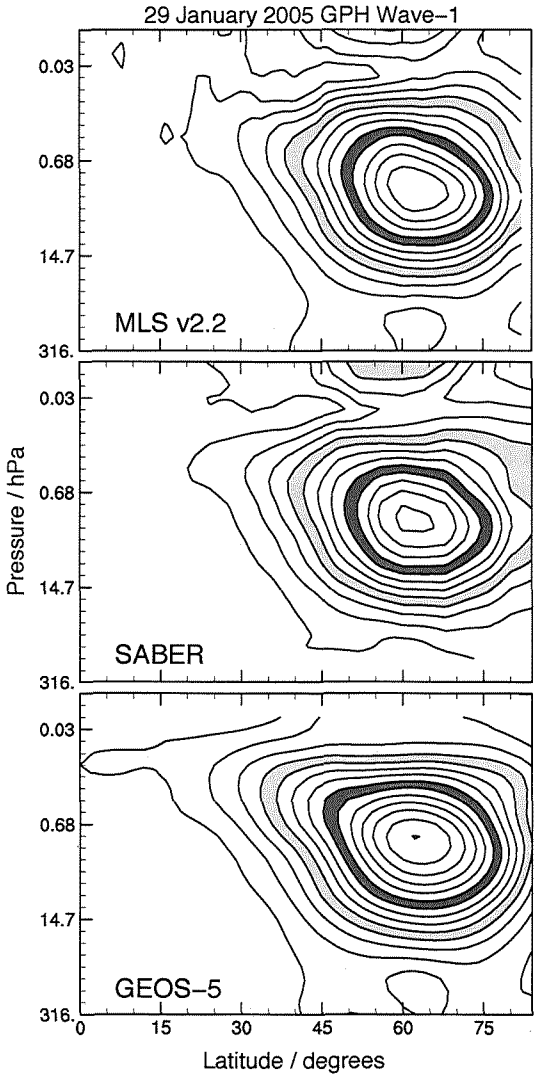

Figure 41. Latitude/pressure sections of MLS, SABER, and GEOS-5 northern hemisphere zonal wavenumber 1 GPH amplitude for 29 January, 2005. Contour interval is 150 m, with light shading for 600–750 m, and dark shading for 1200–1350 m.

ity), can be a powerful tool in helping to assess and improve the behavior of the assimilation systems and their underlying GCMs in this region where data have heretofore been largely unavailable. The ability of the MLS GPH to accurately represent wave motions from the upper troposphere through the mesosphere makes it a useful product for dynamical studies of the middle atmosphere.

4. Conclusions and Future Plans

Version 2.2 of the MLS data processing algorithms produce temperature profiles that are considered scientifically useful at pressures from 316 hPa to 0.001 hPa. In the upper troposphere and lower stratosphere, comparisons of v2.2 temperature with correlative data sets show that MLS has persistent systematic biases with a $\sim$ 3-K peak-to-peak vertical structure. Most of this vertically varying bias is reproduced by a model of MLS amplifier gain compression. The model was in no way tuned to match observed temperature biases but, rather, had its parameters set by laboratory measurements of spare flight-hardware.

The global mean bias relative to eight correlative data sets can be seen in Figure 35 and Figure 36. Between 316 hPa and 10 hPa, most correlative data sets agree with one another within $\sim$ 1 K, and most of the common systematic bias is explained by gain compression (non-linearity) in MLS spectrometer amplifiers which was neglected in the v2.2 instrument forward model.

Table 2 summarizes precision, resolution, observed scatter and modeled and observed biases for temperature. Figure 3 does the same for GPH. The predicted precision and observed scatter of MLS v2.2 temperature is summarized in columns 2 and 3 of Table 2. Column 2 lists retrieval precision that is based upon the propagation of radiance measurement uncertainty through the retrieval software. These precisions range from 0.6 K in the lower stratosphere to 2.5 K in the mesosphere and to 1 K at 316 hPa. Precision can also be estimated from successive views of similar scenes. Column 3 contains the RMS of differences of measurements from successive orbits (divided by the square-root of two, as this is the difference of two noisy signals) for latitudes are seasons where longitudinal variability is small and/or is a function only of local solar time. The RMS of successive-orbit pairs is smallest in high-latitude summer, where atmospheric variability is small, and these values provide an upper bound on measurement precision. These values are reported in column 3 and are slightly larger than those estimated by the measurement system in the troposphere and lower stratosphere and $\sim$ 1.4x larger from the middle stratosphere through the mesosphere. GPH precision estimates from the retrieval system are given in column 2 of Table 3. Values range from $\sim$ 35 m in the stratosphere to $\sim$ 100 m at 0.001 hPa.

The vertical and horizontal resolution of the temperature product is shown in column 4 of Table 2. Vertical resolution is 6 km at 316 hPa, 4 km at 100 hPa, 3 km at 31.6 hPa, 4 km at 10 hPa, 8 km at 3.16 hPa and 13 km at 0.01 hPa. Along-track resolution is 200 km from 316 hPa to 0.316 hPa and degrades to 300 hPa at 0.01 hPa and lower pressures. The across-track beam width is 6–12 km.

The accuracy of the v2.2 temperature measurements has been estimated both by propagating uncertainties in measurement and retrieval parameters, and through comparisons with correlative data sets. Column 5 of Table 2 gives esti-

mates from the propagation of parameter uncertainties. This estimate is broken into two pieces. the first term is due to amplifier "gain compression" and has a known sign. The second term includes spectroscopic parameters, retrieval numerics and pointing, for which the sign of resulting bias is unknown. Gain compression results a global bias profile of -1.5 K to +4.5 K, with significant vertical structure. The simulation suggests that this bias does not have significant latitudinal dependence. Systematic uncertainties of unknown sign are of $\sim$ 2 K magnitude over most of the retrieval range, increasing to 5 k at 316 hPa and to 3 K at 0.001 hPa.

Column 6 contains accuracy estimates based upon observed biases between MLS and collocated correlative profiles from analyses and with other previously-validated satellite-based measurements. In the troposphere and lower stratosphere, the estimated biases are consistent to within $\sim$ 1.5 K between most of the correlative data sets with a vertical oscillation that must be presumed to be in the MLS measurement. This oscillation has an amplitude of 2–3 K and a frequency of about 1.5 cycles per decade of pressure. From 316 hPa to $\sim$10 hPa there is generally agreement to $\sim$ 1 K between the assimilations (ECMWF and GEOS-5) and AIRS, radiosondes and CHAMP, which show consistent biases with respect to MLS. SABER and ACE have generally warm biases of $\sim$ 2 K relative to this group. Figure 36 shows the global mean biases in the left panel and the 1 σ scatter about the mean in the right panel for these eight comparisons. Between 1 hPa and 0.001 hPa, MLS has biases with respect to SABER of +1 K to -5 K between 1 hPa and 0.1 hPa, of 0 K to -3 K between 0.1 K and 0.01 K and increasing in magnitude to -10 K at 0.001 hPa.

The structure and amplitude of tropospheric and stratospheric temperature biases predicted by the gain compression model is in excellent agreement with the observed biases shown in Figure 36 and in Table 2. Gain compression also explains the $\sim$140-m global bias in 100 hPa GPH between MLS and GEOS-5. No parameter tuning was done to achieve this agreement. Integrating a model of gain compression into a future version of the MLS retrieval algorithms is essential to the improvement of temperature retrieval performance. Retrieved temperature, GPH and the associated scan-height – tangent-pressure relationship are the foundation upon which all MLS retrievals are built, so their improvement should lead to more accurate and internally-consistent atmospheric constituent retrievals.

Biases between MLS and correlative measurements in the mesosphere are not well understood. Correction for gain compression will permit the internally-consistent use of more radiances in the retrieval, and will improve vertical resolution of the temperature product in the upper stratosphere and mesosphere.

Elimination of large numbers of convergence failures in temperature retrievals in autumn and early winter poles would be a further goal of a new version, as would the realignment of Status fields to facilitate the flagging of profiles potentially impacted by clouds.

Acknowledgments. Funding for ACE was provided by the Canadian Space Agency and the Natural Sciences and Engineering Research Council (NSERC) of Canada. Work at the Jet Propulsion Laboratory, California Institute of Technology, was done under contract with the National Aeronautics and Space Administration. The ECMWF is thanked for providing their data. CHAMP data was obtained from the http://genesis.jpl.nasa.gov web site, operated and maintained at JPL. Chris Mertens from NASA Langley and the SABER data processing team at GATS, Inc. are thanked for providing SABER data.

We wish to thank the Aura Project for their support throughout the years (before and after Aura launch), in particular M. Schoeberl, A. Douglass (also as co-chair of the Aura validation working group), E. Hilsenrath, and J. Joiner. We also acknowledge the support from NASA Headquarters, P. DeCola for MLS and Aura, and M. Kurylo, J. Gleason, B. Doddridge, and H. Maring, especially in relation to the Aura validation activities and campaign planning efforts. We greatly appreciate the efforts of Bojan Bojkov and the Aura Validation Data Center (AVDC) team, whose work facilitated the MLS validation activities.

References

Aumann, H., et al., *AIRS/AMSU/HSB Version 4.0 Data Release User Guide*, JPL, version 1.0 ed., 2005.

Bernath, P., et al., Atmospheric chemistry experiment(ACE): mission overview, *Proceedings of SPIE, 5542*, 146–156, 2004.

Bloom, S., L. Takacs, A. da Silva, and D. Ledvina, Data Assimilation Using Incremental Analysis Updates, *Monthly Weather Review, 124*, 1256–1271, 1996.

Boone, C., R. Nassar, K. Walker, Y. Rochon, S. McLeod, C. Rinsland, and P. Bernath, Retrievals for the atmospheric chemistry experiment Fourier-transform spectrometer, *Applied Optics, 44*, 7218–7231, 2005.

Brasseur, G., and S. Solmon, *Aeronomy of the Middle Atmosphere*, second edition ed., D. Reidel, Dordrecht, The Netherlands, 1986.

Chahine, M. T., et al., The atmospheric infrared sounder (airs): Improving weather forecasting and providing new data on greenhouse gases, *BAMS*, 2006, in press.

Davies, T., M. J. P. Cullen, A. J. Malcolm, M. H. Mawson, A. Staniforth, A. A. White, and N. Wood, A new dynamical core for the met office's global and regional modelling of the atmosphere, *Q. J. R. Meteorl. Soc., 131*, 1759–1782, 2005.

Divakarla, M., C. Barnet, M. Goldberg, L. McMillin, E. Maddy, W. Wolf, L. Zhou, and X. Liu, Validation of Atmospheric Infrared Sounder temperature and water vapor retrievals with matched radiosonde measurements and forecasts, *Journal of Geophysical Research, 111*, 2006, doi:10.1029/2005JD006116.

Table 2. Summary of MLS temperature product

Region	Precision[a] / K	Observed Scatter[b] / K	Resolution Vert. × Horiz. / km	Modeled Bias uncertainty / K	Observed Bias / K	Comments
<0.001 hPa	—	—	—	—	—	Unsuitable for scientific use
0.001 hPa	±2.5	±3.5	15 × 220	+2±3	-9	
0.01 hPa	±2.2	±3	14 × 185	+2±3	-2 to 0	
0.1 hPa	±2	±2.3	9.1 × 170	+2±2	-8 to 0	
0.316 hPa	±1	±1.5	8.3 × 165	+3±2	-7 to -4	
1 hPa	±1	±1.4	7.9 × 165	+1±2	0 to +5	
3.16 hPa	±0.8	±1	6.2 × 165	+2±2	+1	
10 hPa	±0.6	±1	4.3 × 165	0±2	-1 to 0	
14.7 hPa	±0.6	±1	3.9 × 165	-4±2	0 to +1	
31.6 hPa	±0.6	±1	3.5 × 165	+1±2	-2 to 0	
56.2 hPa	±0.8	±0.8	3.8 × 165	-1±2	-2 to 0	
100 hPa	±0.8	±0.8	5.2 × 165	+2±2	0 to +1	
215 hPa	±1	±1	5.0 × 170	-1.5±4	-2.5 to -1.5	
316 hPa	±1	±1	5.3 × 170	0±5	-2 to 0	
1000 – 383 hPa	—	—	—	—	—	Unsuitable for scientific use

[a]Precision on individual profiles

[b]Precision on individual profiles from successive orbits

Table 3. Summary of MLS GPH product

Region	Precision[a] / meters	Resolution Vert. × Horiz. / km	Modeled Bias uncertainty / m	Observed Bias uncertainty / m	Comments
<0.001 hPa	—	—	—	—	Unsuitable for scientific use
0.001 hPa	±110	15 × 220	+700±150	-450	
0.01 hPa	±85	14 × 185	+600±100	-100	
0.1 hPa	±60	9 × 165	+500±150	0	
1 hPa	±45	8 × 165	+300±100	100	
10 hPa	±35	4.3 × 165	+200±100	100	
100 hPa	±30	5.2 × 165	+150±100	150	
316 hPa	±35	5.3 × 170	+100±150	150	
1000 – 383 hPa	—	—	—	—	Unsuitable for scientific use

[a]Precision on individual profiles

Fetzer, E. J., et al., Global comparisons of upper tropospheric water vapor observations from the microwave limb sounder and atmospheric infrared sounder satellite instruments, in preparation.

FLEMING, E., S. CHANDRA, J. BARNETT, and M. CORNEY, Zonal mean temperature, pressure, zonal wind and geopotential height as functions of latitude, *(A 91-24955 09-46) Advances in Space Research.*, *10*, 11–53, 1990.

Fritts, D. C., and M. J. Alexander, Gravity wave dynamics and effects in the middle atmosphere, *Rev. Geophys.*, *41*, doi: 10.1029/2001RG000106, 2003.

Froidevaux, L., et al., Early validation analyses of atmospheric profiles from EOS MLS on the Aura satellite, *IEEE Trans. Geosci. Remote Sens.*, *44*, 1106–1121, 2006.

Gettelman, A., et al., Validation of Aqua satellite data in the upper troposphere and lower stratosphere with in situ aircraft instruments, *Geophys. Res. Lett*, *31*, 2004, doi:10.1029/2004GL020730.

Hajj, G., et al., CHAMP and SAC-C atmospheric occultation results and intercomparisons, *J. Geophys. Res*, *109*, 2004.

Hervig, M., et al., Validation of temperature measurements from the Halogen Occultation Experiment, *J. Geophys. Res*, *101*, 277–10, 1996.

Kahn, B. H., A. Eldering, A. J. Braverman, E. J. Fetzer, J. H. Jiang, E. Fishbein, and D. L. Wu, Towards the characterization of upper tropospheric clouds using airs and mls observations, *J. Geophys. Res.*, *112*, 2007, doi:10.1029/2006JD007336.

Kerzenmacher, T., et al., Measurements of O 3, NO 2 and Temperature during the 2004 Canadian Arctic ACE Validation Campaign, *GEOPHYSICAL RESEARCH LETTERS*, *32*, L16S07, 2005.

Kutepov, A., A. Feofilov, B. Marshall, L. Gordley, W. Pesnell, R. Goldberg, and J. Russell, SABER temperature observations in the summer polar mesosphere and lower thermosphere: Importance of accounting for the CO 2 nu 2 quanta VV exchange, *Geophysical Research Letters*, *33*, 2006.

Lambrigtsen, B., Calibration of the AIRS microwave instruments, *Geoscience and Remote Sensing, IEEE Transactions on*, *41*, 369–378, 2003.

Limpasuvan, V., D. Wu, M. Schwartz, J. Waters, Q. Wu, and T. Killeen, The two-day wave in EOS MLS temperature and wind measurements during 2004-2005 winter, *Geophys. Res. Lett*, *32*, 2005.

Lin, S., A "Vertically Lagrangian" Finite-Volume Dynamical Core for Global Models, *Monthly Weather Review*, *132*, 2293–2307, 2004.

Livesey, N. J., and W. G. Read, Direct retrieval of line-of-sight atmospheric structure from limb sounding observations, *Geophys. Res. Lett.*, *27*, 891–894, 2000.

Livesey, N. J., and W. V. Snyder, EOS MLS retrieval processes algorithm theoretical basis, *Tech. rep.*, Jet Propulsion Laboratory, 2004, D-16159, available on the MLS web site http://mls.jpl.nasa.gov.

Livesey, N. J., W. V. Snyder, W. G. Read, and P. A. Wagner, Retrieval algorithms for the EOS Microwave Limb Sounder (MLS), *IEEE Trans. Geosci. Remote Sens.*, *44*, 1144–1155, 2006.

Livesey, N. J., et al., EOS MLS version 2.2 Level 2 data quality and description document, *Tech. rep.*, Jet Propulsion Laboratory, 2007a.

Livesey, N. J., et al., Validation of eos microwave limb sounder o^3 and co observations in the upper tropospheric and lower stratospheric, *This issue*, 2007b.

Manney, G. L., et al., Solar occulatation satellite data and derived meteorological products: Sampling issues and comparisons with aura mls data, *JGR*, 2007, in praparation.

McHugh, M., M. Hervig, B. Magill, R. Thompson, E. Remsberg, J. Wrotny, and J. Russell, Improved mesospheric temperature, water vapor and polar mesospheric cloud extinctions from HALOE, *Geophysical Research Letters*, *30*, 23–1, 2003.

McHugh, M., B. Magill, K. Walker, C. Boone, P. Bernath, and J. Russell III, Comparison of atmospheric retrievals from ACE and HALOE, *Geophys. Res. Lett*, *32*, 2005.

McLandress, C., and N. A. McFarlane, Interactions between gravity wave drag and forced stationary planetary waves in the winter northern hemisphere middle atmosphere, *J. Atmos. Sci.*, *50*, 1966–1990, 1993.

Miller, M., and A. Untch, The new ECMWF high resolution forecasting system, in *ECMWF Tenth Workshop on Meteorological Operational Systems*, pp. 14–18 November 2005, 2005, available at http://www.ecmwf.int/newsevents/meetings/workshops/2005/MOS_10/presentations/miller.pdf.

Mlynczak, M., personnal communication, 2007.

Mlynczak, M., and J. Russell, An overview of the SABER experiment for the TIMED mission, *NASA Langley Research Center, Optical Remote Sensing of the Atmosphere,*, 2, 1995.

Pagano, T., H. Aumann, D. Hagan, and K. Overoye, Prelaunch and In-Flight Radiometric Calibration of the Atmospheric Infrared Sounder (AIRS), *IEEE TRANSACTIONS ON GEOSCIENCE AND REMOTE SENSING*, *41*, 265, 2003.

Pawson, S., et al., Geos-5 paper, *JGR*, 2007, in preparation.

Read, W. G., Z. Shippony, M. J. Schwartz, N. J. Livesey, and W. V. Snyder, The clear-sky unpolarized forward model for the EOS Microwave Limb Sounder (MLS), *IEEE Trans. Geosci. Remote Sens.*, *44*, 1367–1379, 2006.

Read, W. G., et al., Eos aura microwave limb sounder upper tropospheric and lower stratospheric humidity validation, *This issue*, 2007a.

Read, W. G., et al., Validation of EOS Microwave Limb Sounder upper tropospheric water vapor and relative humidity products, *This issue*, 2007b.

Reichler, T., M. Dameris, and R. Sausen, Determining the tropopause height from gridded data, *Geophys. Res. Lett.*, *30*, 2042, doi:10.1029/2003GL018240, 2003.

Remsberg, E., G. Lingenfelser, V. Harvey, W. Grose, J. Russell, M. Mlynczak, L. Gordley, and B. Marshall, On the verification of the quality of SABER temperature, geopotential height, and wind fields by comparison with Met Office assimilated analyses, *Journal of Geophysical Research*, *108*, 2003.

Remsberg, E., et al., Comparisons of SABER Temperature Profiles With Rocket, Groundbased, and Satellite Measurements, *American Geophysical Union, Fall Meeting 2002, abstract# SA62B-0405*, 2002.

Rienecker, M., et al., The geos-5 data assimilation system: A documentation of geos-5.0, *Technical Report Series on Global Modeling and Data Assimilation NASA TM 104606, v27*, NASA, 2007.

Rodgers, C. D., *Inverse methods for atmospheric science, theory and practice*, World Scientific, 2000.

Schoeberl, M., N. Center, and M. Greenbelt, The afternoon constellation: a formation of Earth observing systems for the atmosphere and hydrosphere, *Geoscience and Remote Sensing Symposium, 2002. IGARSS'02. 2002 IEEE International, 1*, 2002.

Schoeberl, M. R., et al., Overview of the EOS Aura mission, *IEEE Trans. Geosci. Remote Sens., 44*, 1066–1074, 2006.

Schwartz, M., W. Read, and W. Van Snyder, EOS MLS forward model polarized radiative transfer for Zeeman-split oxygen lines, *IEEE Transactions on Geoscience and Remote Sensing, 44*, 1182–1191, 2006.

Simmons, A., M. Hortal, G. Kelly, A. McNally, A. Untch, and S. Uppala, ECMWF Analyses and Forecasts of Stratospheric Winter Polar Vortex Breakup: September 2002 in the Southern Hemisphere and Related Events., *Journal of Atmospheric Sciences, 62*, 668–689, 2005.

Stajner, I., C. Benson, H. Liu, S. Pawson, N. Brubaker, L.-P.Chang, L. Riishojgaard, and R. Todling, Ice polar stratospheric clouds detected from assimilation of atmospheric infrared sounder data, *Geophys. Res. Lett.*, 2007, submitted.

Stephens, G., et al., THE CLOUDSAT MISSION AND THE A-TRAIN, *Bull. Amer. Meteor. Soc, 83*, 1771–1790, 2002.

Susskind, J., C. Barnet, and J. Blaisdell, Retrieval of atmospheric and surface parameters from AIRS/AMSU/HSB data in the presence of clouds, *Geoscience and Remote Sensing, IEEE Transactions on, 41*, 390–409, 2003.

Susskind, J., C. Barnet, J. Blaisdell, L. Iredell, F. Keita, L. Kouvaris, G. Molnar, and M. Chahine, Accuracy of geophysical parameters derived from Atmospheric Infrared Sounder/Advanced Microwave Sounding Unit as a function of fractional cloud cover, *Journal of Geophysical Research, 111*, 2006.

Swinbank, R., N. B. Ingleby, P. M. Boorman, and R. J. Renshaw, A 3D variational data assimilation system for the stratosphere and troposphere, *Tech. Rep. 71*, Met Office Numerical Weather Prediction Forecasting Research Scientific Paper, 2002.

Swinbank, R., M. Keil, D. R. Jackson, and A. A. Scaife, Stratospheric data assimilation at the met office - progress and plans, in *ECMWF workshop on Modelling and Assimilation for the Stratosphere and Tropopause 23-26-June, 2003*, ECMWF, 2004.

Tobin, D., et al., Atmospheric Radiation Measurement site atmospheric state best estimates for Atmospheric Infrared Sounder temperature and water vapor retrieval validation, *J. Geophys. Res, 111*, 2006.

Waters, J. W., et al., The Earth Observing System Microwave Limb Sounder (EOS MLS) on the Aura satellite, *IEEE Trans. Geosci. Remote Sens., 44*, 1075–1092, 2006.

Wickert, J., T. Schmidt, G. Beyerle, R. König, C. Reigber, and N. Jakowski, The Radio Occultation Experiment aboard CHAMP: Operational Data Analysis and Validation of Vertical Atmospheric Profiles, *JMSJ, 82*, 381–395, 2004.

Wickert, J., et al., Atmosphere sounding by GPS radio occultation: First results from CHAMP, *Geophys. Res. Lett, 28*, 3263–3266, 2001.

Wu, D., et al., Aura mls cloud ice measurements and comparisons with cloudsat and other correlative data, *JGR*, 2007, in preparation.

Wu, W., R. Purser, and D. Parrish, Three-Dimensional Variational Analysis with Spatially Inhomogeneous Covariances, *Monthly Weather Review, 130*, 2905–2916, 2002.

M. J. Schwartz (corresponding author), Jet Propulsion Laboratory, Mail Stop 183–701, 4800 Oak Grove Drive, Pasadena, CA 91109. (e-mail: michael.j.schwartz@jpl.nasa.gov)

This preprint was prepared with AGU's LaTeX macros v5.01, with the extension package 'AGU++' by P. W. Daly, version 1.6b from 1999/08/19.